CHAPTER 6

PARAMETRIC STUDY

6.1 Introduction

An extensive parametric study have been done by using FE simulation techniques to investigate the behaviour of CFSST columns under concentric and eccentric loading conditions. All the columns used in the parametric study had a constant cross-sectional dimension of 450 mm × 450 mm (B mm × D mm), representing a medium size composite column for a typical high-rise structure. These studies have been carried out on CFSST columns with normal to high (30-120 MPa) strength of concrete and structural steel yield strength from 448-707 MPa. Limited studies are available till to date on the behaviour of CFSST columns with high strength concrete and steel. Studies on numerical simulations of CFSST columns are also very limited. As experimental studies are costly and time consuming, so numerical study could be a good alternative, accordingly huge number of CFSST columns were numerically analyzed by taking varying different geometric and mechanical parameters easily. The variables were taken in this study were wide range of concrete compressive strength (f'_c), yield strength of stainless steel (0.2% proof strength $\sigma_{0.2}$), depth-to-steel thickness ratio (D/t), slenderness ratio (L/D) and load eccentricity ratio (e/D).

6.2 Description of Specimens

Total 326 models were developed for the purpose of the parametric study. The columns were designated according to the form of C-30-448-30-0-3, where '30' refers to the column concrete compressive strength of 30 MPa, and the rest of them 448-30-0-5, represents the stainless steel 0.2% proof strength, B/t ratio, eccentricity ratio (e/D) and slenderness (L/D) ratio respectively. In this study concrete strength are used 30 MPa, 45 MPa, 60 MPa, 80 MPa, 100 MPa and 120 MPa. Yield (0.2% proof strength) strength of stainless steel are

used 448 MPa, 497 MPa, 536 MPa, 622 MPa and 707 MPa., Depth to thickness ratio is used 30 (t = 15 mm), 50 (t = 9 mm), 75 (t = 6 mm) and 90 (t =5 mm), Eccentricity ratio is used 0, (e = 0 mm), 0.05 (e = 22.5 mm), 0.10 (e = 45 mm), 0.15 (e = 67.5 mm), 0.2 (e = 90 mm) and 0.25 (e = 112.5 mm) and Slenderness ratio is used 3 (L = 1350 mm), 5 (L = 2250 mm), 10 (L = 4500 mm), 15 (L = 6750 mm) and 20 (L = 9000 mm). The FE models developed as stated in Chapter 3, were used to assess the influence of important geometric and material parameters on the behaviour of CFSST columns. These columns were designed and analyzed during the parametric study to incorporate the effects of several geometric and material parameters that can significantly affect CFSST column behaviour. The efficiency and accuracy of the model were demonstrated through comparisons between the experimental and numerical results of a large number of CFSST column tests, as presented in Chapter 5. The model was found to be capable of tracing a stable load-strain history up to failure with good accuracy for CFSST columns with small and large cross-sections, constructed with normal and high strength concrete, and tested under concentric and eccentric loading conditions.

6.3 Design of Parametric Study

A square column with outer dimensions of 450 mm × 450 mm was selected for the parametric study. Typical cross section and elevation of CFSST column used in the parametric study are shown in Figure 6.1. This type of composite columns might be suitable in the construction work of mid-rise buildings and during the parametric study the effects of several geometric and material parameters that can significantly affect CFSST column behaviour will be clear to us. The geometric variables are percentage of structural steel (tube wall thickness), column slenderness and eccentricity of the applied load. The compressive strength of concrete and grade of stainless steel in CFSST column was used as the material variables in the parametric study. The results of parametric studies are given in Tables 6.1 to 6.5.

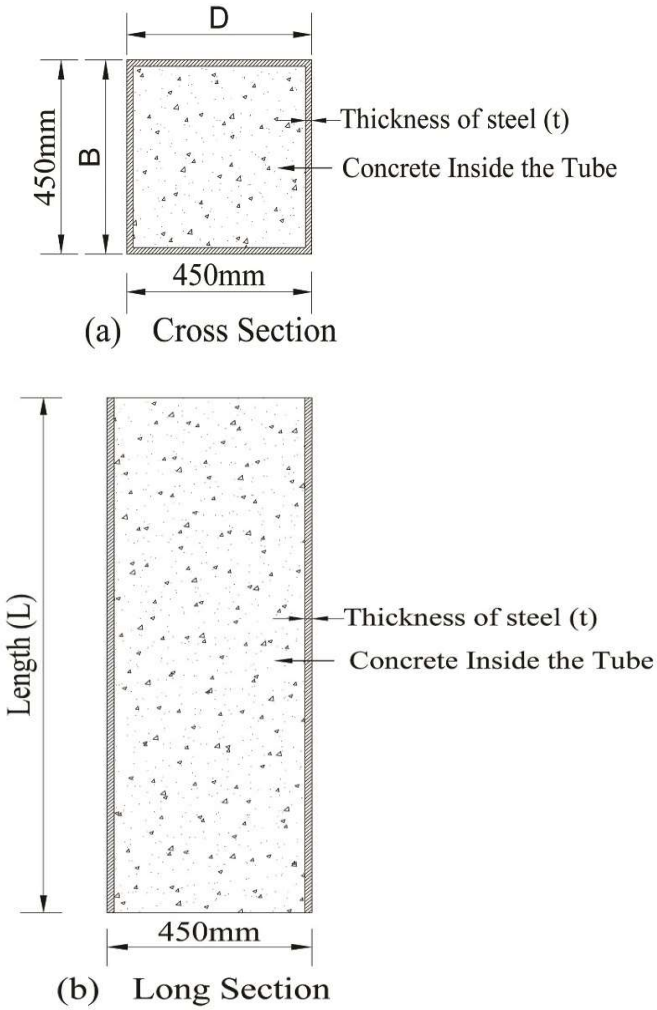

Figure 6.1: Typical cross section and long section of parametric CFSST column
(a) Cross section (b) Long section

6.3.1 Concrete Compressive Strength, (f'_c)

Compressive strength of concrete plays an important role in increasing the load carrying capacity of concrete, thereby reducing the required column size. However, numerical and limited experimental investigations have been performed, till to date, on CFSST columns with high strength concrete. Thus, in the parametric study the concrete strength were varied as 30 MPa, 45 MPa, 60 MPa, 80 MPa, 100 MPa and 120 MPa to investigate the influence of low, medium and high strength concrete in combination with other parameters.

6.3.2 Stain less Steel 0.2% Proof Strength ($\sigma_{0.2}$).

Stainless Steel strength also plays an important role in increasing the load carrying capacity and thereby it reducing the required column size. However, limited experimental and

numerical investigations have been performed, to date, on CFSST columns with high strength steel. In this parametric study the steel strength were varied as 448 MPa, 497 MPa, 536 MPa, 622 MPa, and 707 MPa to investigate the influence of low, medium and high strength steel in combination with other parameters.

6.3.3 Column Depth to Thickness Ratio, (D/t)

The column depth to thickness (D/t) ratio is defined as the ratio of the depth (D), to the thickness (t) of the column cross-section. Four different depth to thickness (D/t) ratio 30, 50, 75 and 90 were employed in the parametric study. These parametric studies were carried out on different concrete compressive strength and steel strength.

6.3.4 Load Eccentricity Ratio, (e/D)

The influence of Load eccentricity ratio of CFSST columns under bending induced by eccentrically applied axial load is greatly affected by the initial load eccentricity ratio. It is obtained by dividing the initial eccentricity, (e), of the applied axial load by the depth of the column cross-section, (D). Higher e/D ratios increase flexural compression in the cross-section. It reduced the load carrying capacity of the column as compared to a concentrically loaded column. The load eccentricity ratios used in this study were 0, 0.05, 0.10, 0.15, 0.20 and 0.25.

6.3.5 Column Slenderness Ratio, (L/D)

The column slenderness ratio is defined as the ratio of the length (L), to the depth of the column cross-section (D). The global stability of the column is controlled by the slenderness L/D) ratio. Three different slenderness ratios 3, 5, 7, 10, 15 and 20 were employed in the parametric study.

6.4 Effect of Concrete Compressive Strength, (f'_c)

In this study, one hundred and twenty (120) columns were simulated to observe the effect of concrete strength using varying the strengths of concrete (30 MPa, 45 MPa, 60 MPa, 80 MPa, 100 MPa and 120 MPa). The result of these 120 columns were divided into Twenty (20) sets (set-1 to 20) for each D/t ratio (90, 75, 50 and 30). Yield strength (0.2% proof strength) of steel for sets were 448 MPa, 497 MPa, 536 MPa, 622 MPa and 707 MPa respectively. This study was done only for concentric load with D/t ratio 90, 75, 50 and 30 (t= 5, 6, 9 and 15 mm) and L/D (L=1350mm) ratios as shown in Table 6.1.

Table 6.1: Effect of Concrete Compressive Strength (f'_c)

Set	Specimen designation	Column Properties				Axial Capacity (kN)		$\frac{P_{AISC}}{P_{FE}}$
		D/t	L/D	f_y (MPa)	f'_c (MPa)	P_{FE}	P_{AISC}	
	C-30-448-90-0-3	90	3	448	30	9160	8924	0.974
	C-45-448-90-0-3	90	3	448	45	11917	11392	0.956
	C-60-448-90-0-3	90	3	448	60	14935	13860	0.928
Set-1	C-80-448-90-0-3	90	3	448	80	19056	17152	0.900
	C-100-448-90-0-3	90	3	448	100	23036	20443	0.887
	C-120-448-90-0-3	90	3	448	120	26073	23734	0.910
	C-30-497-90-0-3	90	3	497	30	9376	9360	0.998
	C-45-497-90-0-3	90	3	497	45	12103	11828	0.977
	C-60-497-90-0-3	90	3	497	60	15311	14296	0.934
Set-2	C-80-497-90-0-3	90	3	497	80	19394	17588	0.907
	C-100-497-90-0-3	90	3	497	100	22636	20879	0.922
	C-120-497-90-0-3	90	3	497	120	24549	24170	0.985
	C-30-536-90-0-3	90	3	536	30	9853	9707	0.985
	C-45-536-90-0-3	90	3	536	45	12667	12176	0.961
	C-60-536-90-0-3	90	3	536	60	15694	14644	0.933
Set-3	C-80-536-90-0-3	90	3	536	80	19295	17935	0.930
	C-100-536-90-0-3	90	3	536	100	23573	21226	0.900
	C-120-536-90-0-3	90	3	536	120	27486	24518	0.892
	C-30-622-90-0-3	90	3	622	30	10074	10473	1.040
	C-45-622-90-0-3	90	3	622	45	13012	12941	0.995
	C-60-622-90-0-3	90	3	622	60	16043	15409	0.961
Set-4	C-80-622-90-0-3	90	3	622	80	20061	18701	0.932
	C-100-622-90-0-3	90	3	622	100	23050	21992	0.954
	C-120-622-90-0-3	90	3	622	120	27532	25283	0.918
	C-30-707-90-0-3	90	3	707	30	10664	11229	1.053
	C-45-707-90-0-3	90	3	707	45	13533	13698	1.012
	C-60-707-90-0-3	90	3	707	60	16553	16166	0.977
Set-5	C-80-707-90-0-3	90	3	707	80	19984	19457	0.974
	C-100-707-90-0-3	90	3	707	100	24601	22748	0.925
	C-120-707-90-0-3	90	3	707	120	28738	26040	0.906

Table 6.1: Effect of Concrete Compressive Strength (f'_c)

Set	Specimen designation	Column Properties				Axial Capacity (kN)		$\frac{P_{AISC}}{P_{FE}}$
		D/t	L/D	f_y (MPa)	f'_c (MPa)	P_{FE}	P_{AISC}	
Set-6	C-30-448-75-0-3	75	3	448	30	10176	9666	0.950
	C-45-448-75-0-3	75	3	448	45	13056	12112	0.928
	C-60-448-75-0-3	75	3	448	60	15952	14558	0.913
	C-80-448-75-0-3	75	3	448	80	19857	17819	0.897
	C-100-448-75-0-3	75	3	448	100	23177	21081	0.910
	C-120-448-75-0-3	75	3	448	120	26799	24342	0.908
Set-7	C-30-497-75-0-3	75	3	497	30	10232	10188	0.996
	C-45-497-75-0-3	75	3	497	45	13138	12634	0.962
	C-60-497-75-0-3	75	3	497	60	16015	15080	0.942
	C-80-497-75-0-3	75	3	497	80	19970	18341	0.918
	C-100-497-75-0-3	75	3	497	100	23497	21603	0.919
	C-120-497-75-0-3	75	3	497	120	26901	24864	0.924
Set-8	C-30-536-75-0-3	75	3	536	30	10860	10604	0.976
	C-45-536-75-0-3	75	3	536	45	13742	13050	0.950
	C-60-536-75-0-3	75	3	536	60	16748	15496	0.925
	C-80-536-75-0-3	75	3	536	80	20651	18757	0.908
	C-100-536-75-0-3	75	3	536	100	24328	22018	0.905
	C-120-536-75-0-3	75	3	536	120	27947	25280	0.905
Set-9	C-30-622-75-0-3	75	3	622	30	11269	11520	1.040
	C-45-622-75-0-3	75	3	622	45	14060	13966	0.995
	C-60-622-75-0-3	75	3	622	60	16924	16412	0.961
	C-80-622-75-0-3	75	3	622	80	21152	19673	0.932
	C-100-622-75-0-3	75	3	622	100	24829	22935	0.954
	C-120-622-75-0-3	75	3	622	120	28904	26196	0.918
Set-10	C-30-707-75-0-3	75	3	707	30	11964	12426	1.039
	C-45-707-75-0-3	75	3	707	45	14865	14872	1.000
	C-60-707-75-0-3	75	3	707	60	17699	17318	0.978
	C-80-707-75-0-3	75	3	707	80	21746	20579	0.946
	C-100-707-75-0-3	75	3	707	100	25298	23841	0.942
	C-120-707-75-0-3	75	3	707	120	29448	27102	0.920

Table 6.1: Effect of Concrete Compressive Strength (f'_c)

Set	Specimen designation	Column Properties				Axial Capacity (kN)		$\frac{P_{AISC}}{P_{FE}}$
		D/t	L/D	f_y (MPa)	f'_c (MPa)	P_{FE}	P_{AISC}	
Set-11	C-30-448-50-0-3	50	3	448	30	12993	11871	0.914
	C-45-448-50-0-3	50	3	448	45	15800	14251	0.902
	C-60-448-50-0-3	50	3	448	60	18587	16630	0.895
	C-80-448-50-0-3	50	3	448	80	22255	19803	0.890
	C-100-448-50-0-3	50	3	448	100	26068	22975	0.881
	C-120-448-50-0-3	50	3	448	120	27851	26148	0.939
Set-12	C-30-497-50-0-3	50	3	497	30	13738	12649	0.921
	C-45-497-50-0-3	50	3	497	45	16567	15029	0.907
	C-60-497-50-0-3	50	3	497	60	19389	17408	0.898
	C-80-497-50-0-3	50	3	497	80	23099	20581	0.891
	C-100-497-50-0-3	50	3	497	100	26556	23753	0.894
	C-120-497-50-0-3	50	3	497	120	29465	26926	0.914
Set-13	C-30-536-50-0-3	50	3	536	30	14444	13268	0.919
	C-45-536-50-0-3	50	3	536	45	17169	15648	0.911
	C-60-536-50-0-3	50	3	536	60	20037	18027	0.900
	C-80-536-50-0-3	50	3	536	80	23745	21200	0.893
	C-100-536-50-0-3	50	3	536	100	27258	24373	0.894
	C-120-536-50-0-3	50	3	536	120	30522	27545	0.902
Set-14	C-30-622-50-0-3	50	3	622	30	15959	14634	0.917
	C-45-622-50-0-3	50	3	622	45	18501	17013	0.920
	C-60-622-50-0-3	50	3	622	60	20952	19393	0.926
	C-80-622-50-0-3	50	3	622	80	24500	22565	0.921
	C-100-622-50-0-3	50	3	622	100	28707	25738	0.897
	C-120-622-50-0-3	50	3	622	120	32162	28911	0.899
Set-15	C-30-707-50-0-3	50	3	707	30	17107	15983	0.934
	C-45-707-50-0-3	50	3	707	45	19867	18363	0.924
	C-60-707-50-0-3	50	3	707	60	22426	20742	0.925
	C-80-707-50-0-3	50	3	707	80	26389	23915	0.906
	C-100-707-50-0-3	50	3	707	100	29687	27087	0.912
	C-120-707-50-0-3	50	3	707	120	33668	30260	0.899

Table 6.1: Effect of Concrete Compressive Strength (f'_c)

Set	Specimen designation	Column Properties				Axial Capacity (kN)		$\frac{P_{AISC}}{P_{FE}}$
		D/t	L/D	f_y (MPa)	f'_c (MPa)	P_{FE}	P_{AISC}	
Set-16	C-30-448-30-0-3	30	3	448	30	18022	16191	0.898
	C-45-448-30-0-3	30	3	448	45	20508	18440	0.899
	C-60-448-30-0-3	30	3	448	60	22834	20689	0.906
	C-80-448-30-0-3	30	3	448	80	26335	23688	0.899
	C-100-448-30-0-3	30	3	448	100	29866	26687	0.894
	C-120-448-30-0-3	30	3	448	120	33501	29686	0.886
Set-17	C-30-497-30-0-3	30	3	497	30	19384	17470	0.901
	C-45-497-30-0-3	30	3	497	45	21881	19719	0.901
	C-60-497-30-0-3	30	3	497	60	24303	21968	0.904
	C-80-497-30-0-3	30	3	497	80	27464	24967	0.909
	C-100-497-30-0-3	30	3	497	100	30570	27966	0.915
	C-120-497-30-0-3	30	3	497	120	34782	30965	0.890
Set-18	C-30-536-30-0-3	30	3	536	30	20502	18488	0.902
	C-45-536-30-0-3	30	3	536	45	23017	20737	0.901
	C-60-536-30-0-3	30	3	536	60	25489	22986	0.902
	C-80-536-30-0-3	30	3	536	80	28616	25985	0.908
	C-100-536-30-0-3	30	3	536	100	31786	28984	0.912
	C-120-536-30-0-3	30	3	536	120	34882	31982	0.917
Set-19	C-30-622-30-0-3	30	3	622	30	22936	20732	0.904
	C-45-622-30-0-3	30	3	622	45	25418	22982	0.904
	C-60-622-30-0-3	30	3	622	60	27764	25231	0.909
	C-80-622-30-0-3	30	3	622	80	31051	28229	0.909
	C-100-622-30-0-3	30	3	622	100	34279	31228	0.911
	C-120-622-30-0-3	30	3	622	120	37420	34227	0.915
Set-20	C-30-707-30-0-3	30	3	707	30	25408	22951	0.903
	C-45-707-30-0-3	30	3	707	45	27799	25200	0.907
	C-60-707-30-0-3	30	3	707	60	30101	27449	0.912
	C-80-707-30-0-3	30	3	707	80	33391	30448	0.912
	C-100-707-30-0-3	30	3	707	100	36670	33447	0.912
	C-120-707-30-0-3	30	3	707	120	39849	36446	0.915

6.4.1 Load versus Average Axial Deformation Response

Figures 6.2a, 6.2b, 6.2c, 6.2d and 6.2e represent the axial load versus deformation curves of the columns in Set-1, Set-2, Set-3, Set-4 and Set-5. It was observed from these Figures that the ultimate axial load and stiffness of the CFSST column is greatly influenced by the strength of concrete. The axial load versus axial deformation responses of CFSST columns with higher strength concrete show steeper slopes at the ascending portions of the curves due to the higher modulus of elasticity. Columns (C_80_448_90_0_3, C_100_448_90_0_3 and C_120_448_90_0_3) constructed with 80, 100 & 120 MPa concrete also demonstrate sharp post peak strength declines as compared to other columns. However, the columns constructed with higher strength concrete showed brittle failure manner as compared to column with medium and lower strength of concrete.

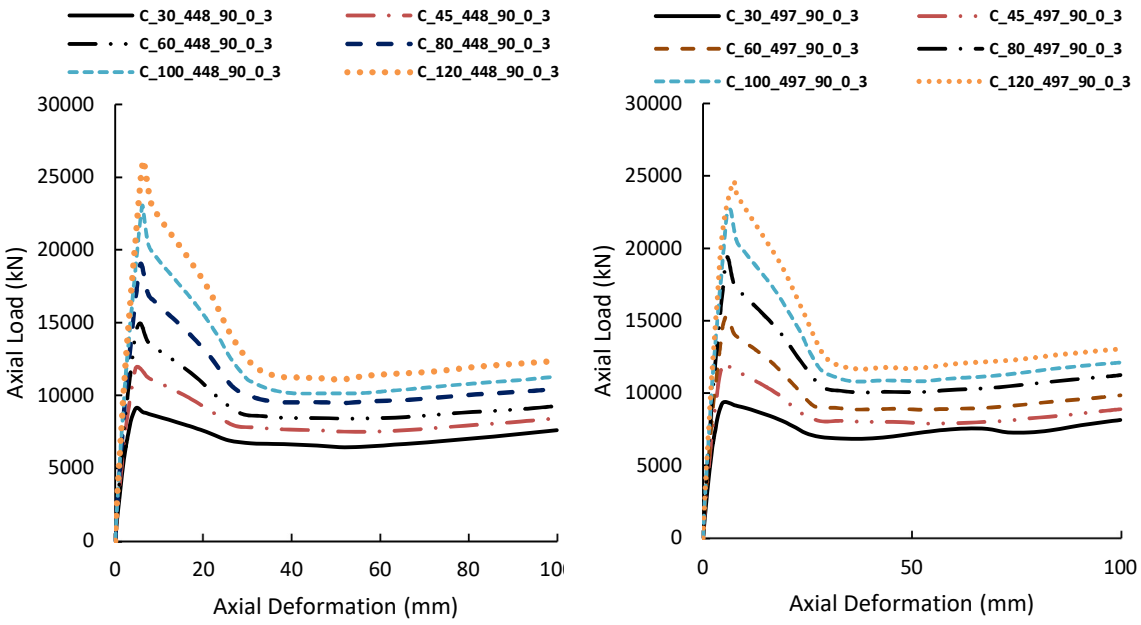

(a) **(b)**

Figure 6.2: Effect of Concrete Strength, (a) Effect of concrete strength on axial load vs axial deformation curve (Set-1); (b) Effect of concrete strength on axial load vs axial deformation curve (Set-2).

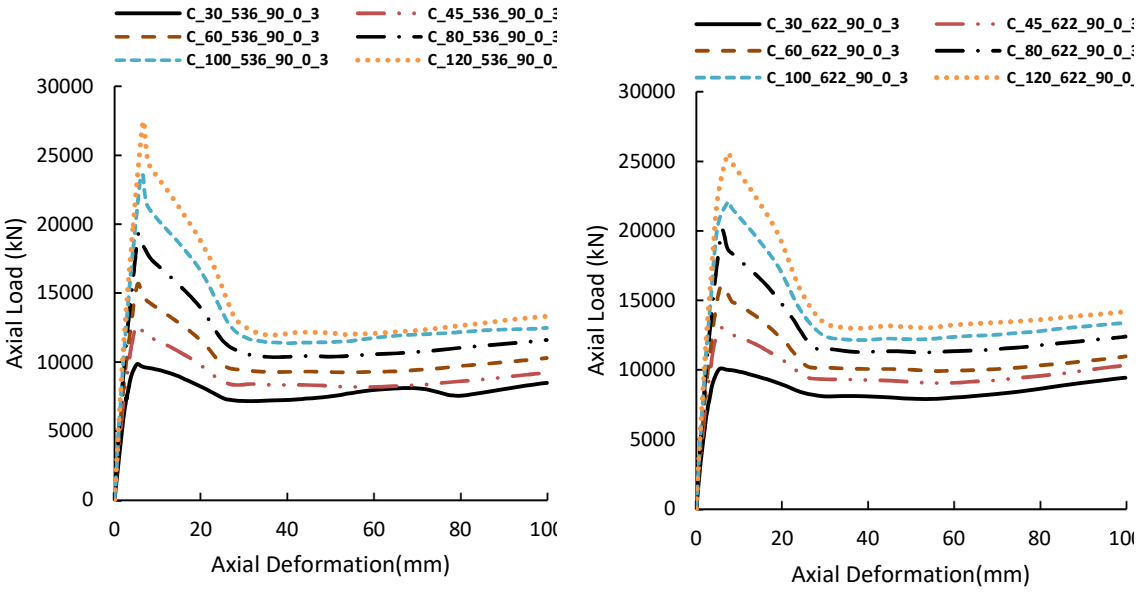

(c) **(d)**

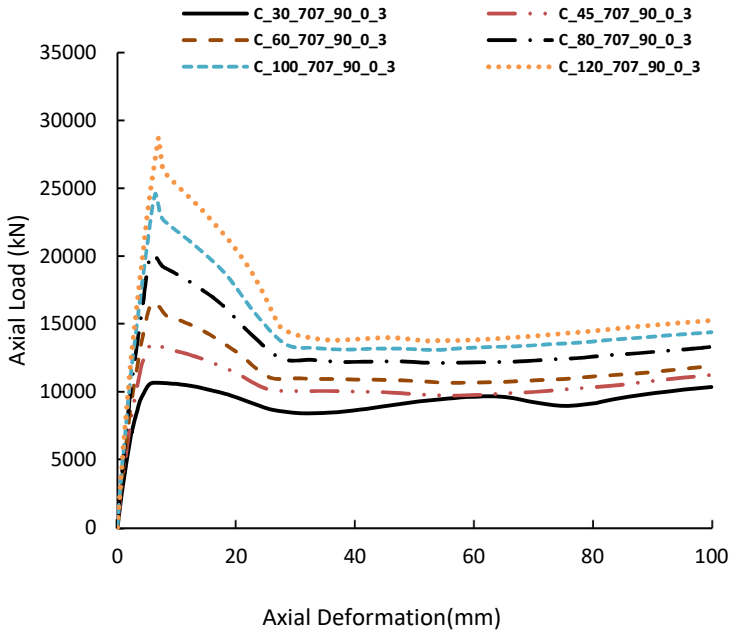

(e)

Figure 6.2: Effect of Concrete Strength, (c) Effect of concrete strength on axial load vs axial deformation curve (Set-3); (d) Effect of concrete strength on axial load vs axial deformation curve (Set-4); (e) Effect of concrete strength on axial load vs axial deformation curve (Set-5)

6.4.2 Comparison of Peak Load

It is observed from Table 6:1a that the axial capacity of column C-45-448-90-0-3, C-60-448-90-0-3, C-80-448-90-0-3, C-100-448-90-0-3 and C-120-448-90-0-3 are increased by 30%, 63%, 108%, 151% and 184% with the increment of concrete strength 50% 100%, 166%, 233% and 300% (Concrete Strength increment from 30 MPa to 45, 60, 80, 100 and120 MPa Respectively) than column C-30-448-90-0-3. On the other hand, code (AISC-LRFD 2010) predicted capacity increment were also increased 27%, 55%, 92%, 129% and 166%, respectively.

Similarly, the axial capacity of column C-45-536-90-0-3, C-60-536-90-0-3, C-80-536-90-0-3, C-100-536-90-0-3 and C-45-536-90-0-3 are increased by 28%, 59%, 96%, 139% and 177% with the increment of concrete strength 50% 100%, 166%, 233% and 300% (Concrete Strength increment from 30 MPa to 45, 60, 80, 100 and120 MPa Respectively) than column C-30-536-90-0-3. On the other hand, code (AISC-LRFD 2010) predicted capacity increment were also 25%, 50%, 85%, 119% and 153%, respectively.

Axial capacity of column increment rate was higher due to variation of concrete strength with lower grade steel. With the increasing of steel strength, the axial capacity increment rate was comparatively lower with same concrete strength. The code (AISC-LRFD 2010) predicted capacity behaviour was also same with the numerical bahaviour.

6.4.3 Modes of Failure

The failures in the columns occurred by crushing of concrete followed by yielding of steel. The crushing of concrete (CC) started near the middle of the columns. The deformed shape with stress contour at failure of concrete was captured as shown in Figure 6.3a and 6.3b similarly the contour at failure of stainless steel was captured as shown in Figure 6.3c and overall failure deformed shape shown as Figure 6.3d. From the all figures it is observed that Von Mises stress failure (yield) of the structural steel and concrete of column was started near the middle of the columns.

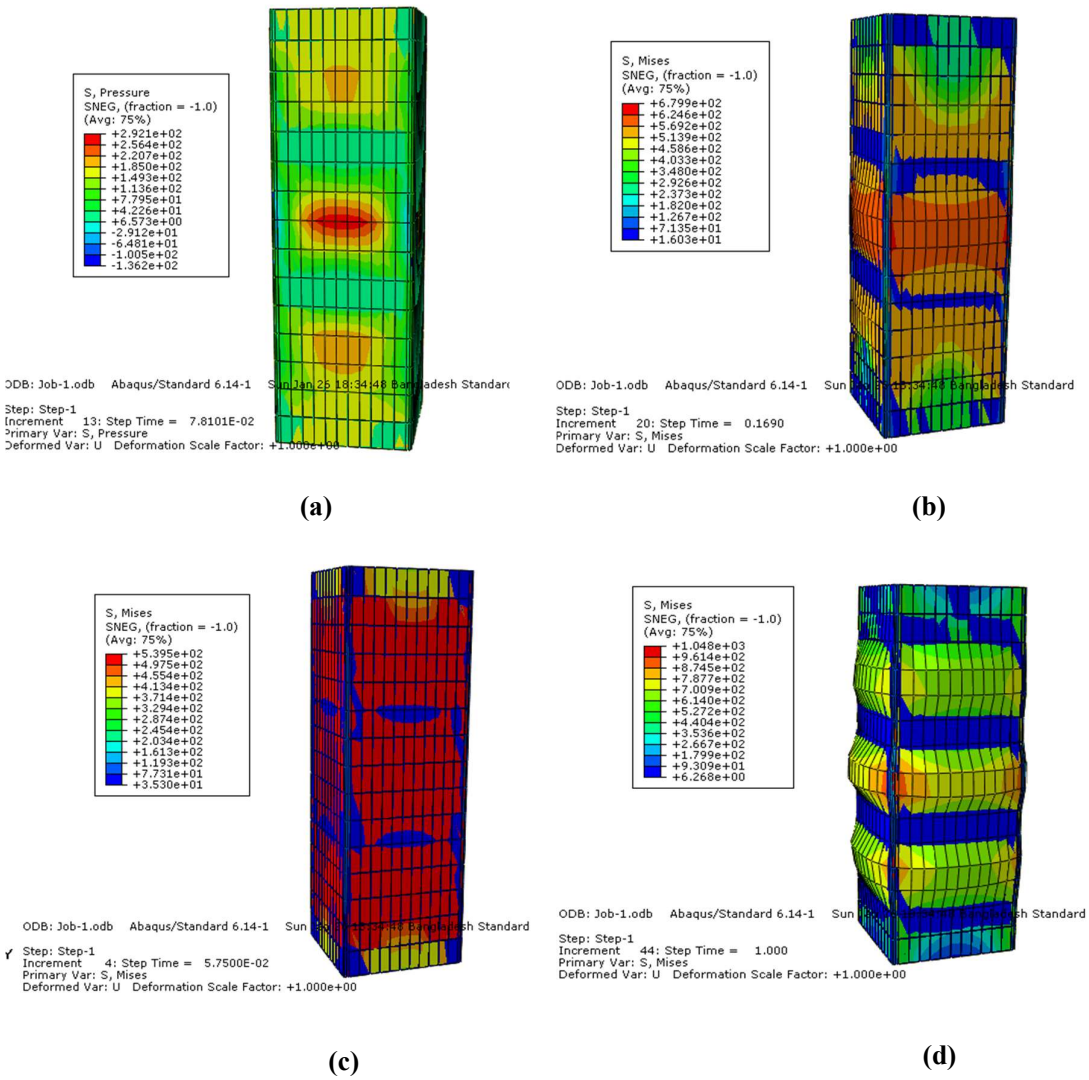

Figure 6.3: Stress contour of steel at failure, (a) & (b) Stress contour of concrete at failure; (c) Stress contour of steel at failure; (d) Overall failure.

6.5 Effect of Steel Yield Strength (0.2% Proof Strength $\sigma_{0.2}$)

In this study, one hundred fifty (150) columns were simulated to observe the effect of steel strength using varying the strengths of steel (448 MPa, 497 MPa, 536 MPa 622 MPa, and 707 MPa). The results of observed columns were divided into 24 sets (set-21 to 44) shown in Table 6.2 for varying steel strength as well as concrete strength (30 MPa, 45 MPa, 60 MPa, 80 MPa, 100MPa and 120 MPa. This study was done only for concentric load with constant D/t (t = 5 mm) and L/D (L=1350 mm) ratios.

Table 6.2: Effect Of Stainless Steel Yield Strength ($\sigma_{0.2}$)

Set	Specimen designation	Column Properties				Axial Capacity (kN)		$\frac{P_{AISC}}{P_{FE}}$
		D/t	L/D	f_y (MPa)	f'_c (MPa)	P_{FE}	P_{AISC}	
Set-21	C-30-448-90-0-3	90	3	448	30	9160	8924	0.974
	C-30-497-90-0-3	90	3	497	30	9376	9360	0.998
	C-30-536-90-0-3	90	3	536	30	9853	9707	0.961
	C-30-622-90-0-3	90	3	622	30	10074	10473	1.04
	C-30-707-90-0-3	90	3	707	30	10664	11229	1.053
Set-22	C-45-448-90-0-3	90	3	448	45	11917	11392	0.956
	C-45-497-90-0-3	90	3	497	45	12103	11828	0.977
	C-45-536-90-0-3	90	3	536	45	12667	12176	0.961
	C-45-622-90-0-3	90	3	622	45	13012	12941	0.995
	C-45-707-90-0-3	90	3	707	45	13533	13698	1.01
Set-23	C-60-448-90-0-3	90	3	448	60	14935	13860	0.928
	C-60-497-90-0-3	90	3	497	60	15311	14296	0.934
	C-60-536-90-0-3	90	3	536	60	15694	14644	0.933
	C-60-622-90-0-3	90	3	622	60	16043	15409	0.961
	C-60-707-90-0-3	90	3	707	60	16553	16166	0.977
Set-24	C-80-448-90-0-3	90	3	448	80	19056	17152	0.900
	C-80-497-90-0-3	90	3	497	80	19394	17588	0.907
	C-80-536-90-0-3	90	3	536	80	19695	17935	0.91
	C-80-622-90-0-3	90	3	622	80	20061	18701	0.932
	C-80-707-90-0-3	90	3	707	80	19984	19457	0.974
Set-25	C-100-448-90-0-3	90	3	448	100	22636	20443	0.887
	C-100-497-90-0-3	90	3	497	100	23036	20879	0.922
	C-100-536-90-0-3	90	3	536	100	23573	21226	0.90
	C-100-622-90-0-3	90	3	622	100	23750	21993	0.926
	C-100-707-90-0-3	90	3	707	100	24601	22748	0.925
Set-26	C-120-448-90-0-3	90	3	448	120	24549	23734	0.91
	C-120-497-90-0-3	90	3	497	120	26073	24170	0.985
	C-120-536-90-0-3	90	3	536	120	27486	24518	0.892
	C-120-622-90-0-3	90	3	622	120	27992	25283	0.918
	C-120-707-90-0-3	90	3	707	120	28738	26040	0.906

Table 6.2: Effect Of Stainless Steel Yield Strength ($\sigma_{0.2}$)

Set	Specimen designation	Column Properties				Axial Capacity (kN)		$\frac{P_{AISC}}{P_{FE}}$
		D/t	L/D	f_y (MPa)	f'_c (MPa)	P_{FE}	P_{AISC}	
Set-27	C-30-448-75-0-3	75	3	448	30	10176	9666	0.950
	C-30-497-75-0-3	75	3	497	30	10232	10188	0.996
	C-30-536-75-0-3	75	3	536	30	10860	10604	0.976
	C-30-622-75-0-3	75	3	622	30	11269	11520	1.022
	C-30-707-75-0-3	75	3	707	30	11964	12426	1.039
Set-28	C-45-448-75-0-3	75	3	448	45	13056	12112	0.928
	C-45-497-75-0-3	75	3	497	45	13138	12634	0.962
	C-45-536-75-0-3	75	3	536	45	13742	13050	0.950
	C-45-622-75-0-3	75	3	622	45	14060	13966	0.993
	C-45-707-75-0-3	75	3	707	45	14865	14872	1.000
Set-29	C-60-448-75-0-3	75	3	448	60	15952	14558	0.913
	C-60-497-75-0-3	75	3	497	60	16015	15080	0.942
	C-60-536-75-0-3	75	3	536	60	16748	15496	0.925
	C-60-622-75-0-3	75	3	622	60	16924	16412	0.970
	C-60-707-75-0-3	75	3	707	60	17699	17318	0.978
Set-30	C-80-448-75-0-3	75	3	448	80	19857	17819	0.897
	C-80-497-75-0-3	75	3	497	80	19970	18341	0.918
	C-80-536-75-0-3	75	3	536	80	20651	18757	0.908
	C-80-622-75-0-3	75	3	622	80	21152	19673	0.930
	C-80-707-75-0-3	75	3	707	80	21746	20579	0.946
Set-31	C-100-448-75-0-3	75	3	448	100	23177	21081	0.910
	C-100-497-75-0-3	75	3	497	100	23497	21603	0.919
	C-100-536-75-0-3	75	3	536	100	24328	22018	0.905
	C-100-622-75-0-3	75	3	622	100	24829	22935	0.924
	C-100-707-75-0-3	75	3	707	100	25298	23841	0.942
Set-32	C-120-448-75-0-3	75	3	448	120	26799	24342	0.908
	C-120-497-75-0-3	75	3	497	120	26901	24864	0.924
	C-120-536-75-0-3	75	3	536	120	27947	25280	0.905
	C-120-622-75-0-3	75	3	622	120	28904	26196	0.906
	C-120-707-75-0-3	75	3	707	120	29448	27102	0.920

Table 6.2: Effect Of Stainless Steel Yield Strength ($\sigma_{0.2}$)

Set	Specimen designation	Column Properties				Axial Capacity (kN)		$\frac{P_{AISC}}{P_{FE}}$
		D/t	L/D	f_y (MPa)	f'_c (MPa)	P_{FE}	P_{AISC}	
Set-33	C-30-448-50-0-3	50	3	448	30	12993	11871	0.914
	C-30-497-50-0-3	50	3	497	30	13738	12649	0.921
	C-30-536-50-0-3	50	3	536	30	14444	13268	0.919
	C-30-622-50-0-3	50	3	622	30	15959	14634	0.917
	C-30-707-50-0-3	50	3	707	30	17107	15983	0.934
Set-34	C-45-448-50-0-3	50	3	448	45	15800	14251	0.902
	C-45-497-50-0-3	50	3	497	45	16567	15029	0.907
	C-45-536-50-0-3	50	3	536	45	17169	15648	0.911
	C-45-622-50-0-3	50	3	622	45	18501	17013	0.920
	C-45-707-50-0-3	50	3	707	45	19867	18363	0.924
Set-35	C-60-448-50-0-3	50	3	448	60	18587	16630	0.895
	C-60-497-50-0-3	50	3	497	60	19389	17408	0.898
	C-60-536-50-0-3	50	3	536	60	20037	18027	0.900
	C-60-622-50-0-3	50	3	622	60	20952	19393	0.926
	C-60-707-50-0-3	50	3	707	60	22426	20742	0.925
Set-36	C-80-448-50-0-3	50	3	448	80	22255	19803	0.890
	C-80-497-50-0-3	50	3	497	80	23099	20581	0.891
	C-80-536-50-0-3	50	3	536	80	23745	21200	0.893
	C-80-622-50-0-3	50	3	622	80	24500	22565	0.921
	C-80-707-50-0-3	50	3	707	80	26389	23915	0.906
Set-37	C-100-448-50-0-3	50	3	448	100	26068	22975	0.881
	C-100-497-50-0-3	50	3	497	100	26556	23753	0.894
	C-100-536-50-0-3	50	3	536	100	27258	24373	0.894
	C-100-622-50-0-3	50	3	622	100	28707	25738	0.897
	C-100-707-50-0-3	50	3	707	100	29687	27087	0.912
Set-38	C-120-448-50-0-3	50	3	448	120	27851	26148	0.939
	C-120-497-50-0-3	50	3	497	120	29465	26926	0.914
	C-120-536-50-0-3	50	3	536	120	30522	27545	0.902
	C-120-622-50-0-3	50	3	622	120	32162	28911	0.899
	C-120-707-50-0-3	50	3	707	120	33668	30260	0.899

Table 6.2: Effect Of Stainless Steel Yield Strength ($\sigma_{0.2}$)

Set	Specimen designation	Column Properties				Axial Capacity (kN)		$\frac{P_{AISC}}{P_{FE}}$
		D/t	L/D	f_y (MPa)	f'_c (MPa)	P_{FE}	P_{AISC}	
Set-39	C-30-448-30-0-3	30	3	448	30	18022	16191	0.898
	C-30-497-30-0-3	30	3	497	30	19383	17470	0.901
	C-30-536-30-0-3	30	3	536	30	20502	18488	0.902
	C-30-622-30-0-3	30	3	622	30	22936	20732	0.904
	C-30-707-30-0-3	30	3	707	30	25408	22951	0.903
Set-40	C-45-448-30-0-3	30	3	448	45	20508	18440	0.899
	C-45-497-30-0-3	30	3	497	45	21887	19719	0.901
	C-45-536-30-0-3	30	3	536	45	23017	20737	0.901
	C-45-622-30-0-3	30	3	622	45	25418	22982	0.904
	C-45-707-30-0-3	30	3	707	45	27799	25200	0.907
Set-41	C-60-448-30-0-3	30	3	448	60	22843	20689	0.906
	C-60-497-30-0-3	30	3	497	60	24303	21968	0.904
	C-60-536-30-0-3	30	3	536	60	25489	22986	0.902
	C-60-622-30-0-3	30	3	622	60	27764	25231	0.909
	C-60-707-30-0-3	30	3	707	60	30101	27449	0.912
Set-42	C-80-448-30-0-3	30	3	448	80	26335	23688	0.899
	C-80-497-30-0-3	30	3	497	80	27464	24967	0.909
	C-80-536-30-0-3	30	3	536	80	28616	25985	0.908
	C-80-622-30-0-3	30	3	622	80	31051	28229	0.909
	C-80-707-30-0-3	30	3	707	80	33391	30448	0.912
Set-43	C-100-448-30-0-3	30	3	448	100	28866	26687	0.925
	C-100-497-30-0-3	30	3	497	100	30570	27966	0.915
	C-100-536-30-0-3	30	3	536	100	31786	28984	0.912
	C-100-622-30-0-3	30	3	622	100	34279	31228	0.911
	C-100-707-30-0-3	30	3	707	100	36670	33447	0.912
Set-44	C-120-448-30-0-3	30	3	448	120	33501	29686	0.886
	C-120-497-30-0-3	30	3	497	120	34782	30965	0.890
	C-120-536-30-0-3	30	3	536	120	35882	31982	0.917
	C-120-622-30-0-3	30	3	622	120	37420	34227	0.915
	C-120-707-30-0-3	30	3	707	120	39849	36446	0.915

6.5.1 Load versus Average Axial Deformation Response

Figures 6.4a, 6.4b, 6.4c, 6.4d, 6.4e and 6.4f shows the effects of structural steel strength on the axial load versus axial deformation responses for columns of Set-21, Set-22, Set-23, Set-24, Set-25 and Set-26 respectively. It is apparent from the figures that as the steel strength is increased the stiffness and the ultimate capacity of CFSST column increases. The residual strength after failure and ductility of the columns were also observed to increase significantly with the increase in the steel strength. This behaviour observed for columns are inserted below.

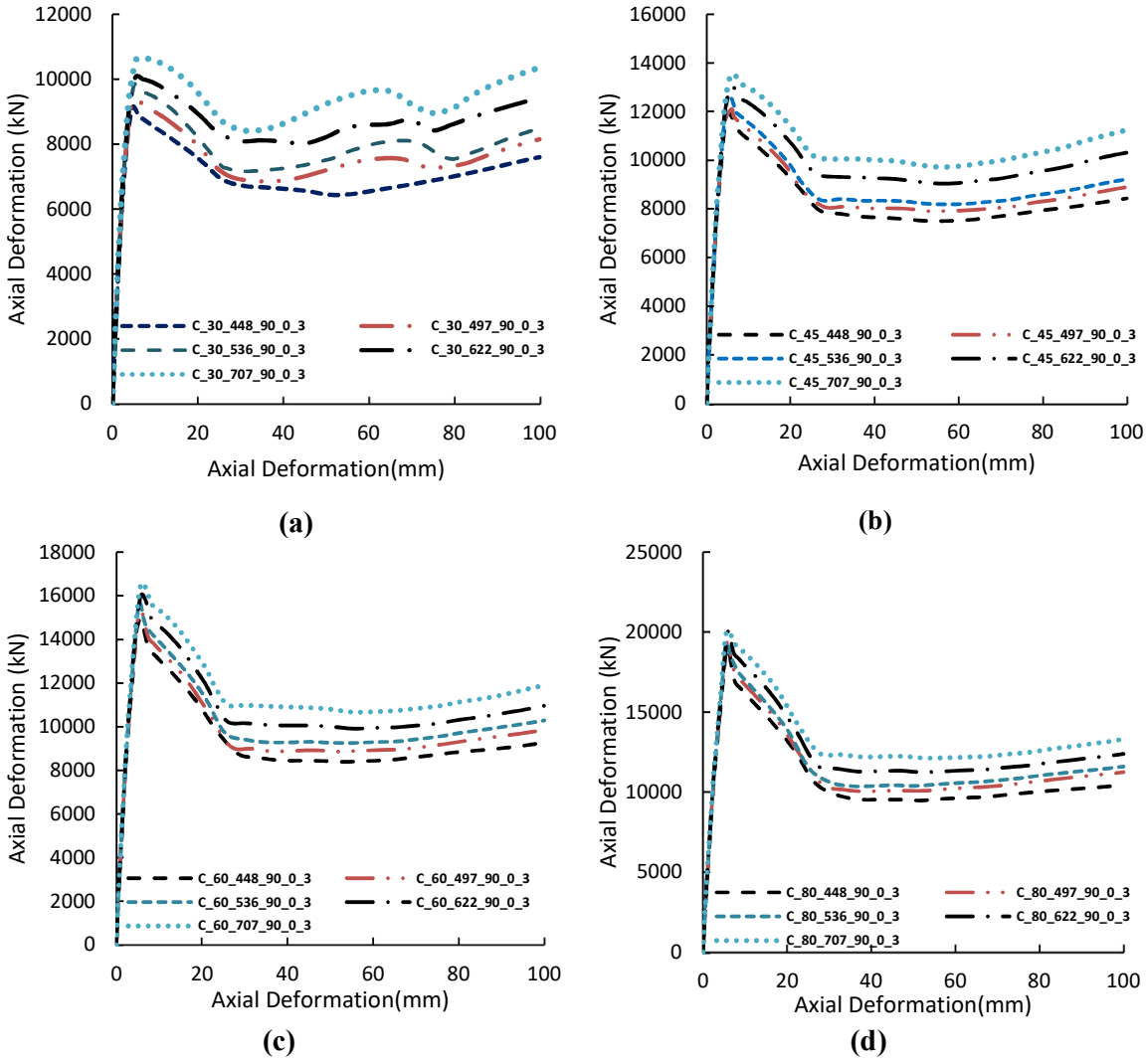

Figure 6.4: Effect of yield strength of stainless-steel strength, (a) axial load vs axial deformation curve (Set-21); (b) axial load vs axial deformation curve (Set-22); (c) axial load vs axial deformation curve (Set-23); (d) axial load vs axial deformation curve (Set-24)

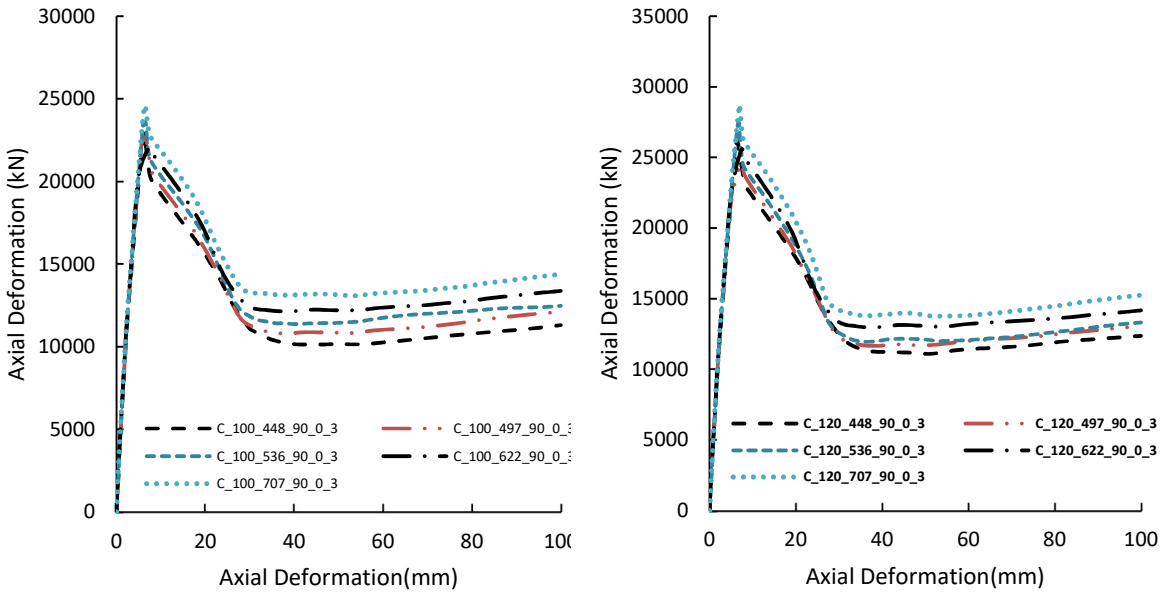

(e) **(f)**

Figure 6.4: Effect of Stainless-Steel Strength, (e) axial load vs axial deformation curve (Set-25); (f) axial load vs axial deformation curve (Set-26)

6.5.2 Comparison of Peak Load

It is observed from Table 6:3a where D/t=90 and f'_c=30 MPa, the axial capacity of column C-30-497-90-0-3, C-30-536-90-0-3, C-30-622-90-0-3 and C-30-707-90-0-3 are increased by 3%, 7%, 10% and 16% than column C-30-448-90-0-3 with the increment of proof steel strength 11%, 20%, 39% and 58% respectively. On the other and, code (AISC-LRFD 2010) predicted capacity increment were 4%, 8%,16% and 25%, respectively.

Again when D/t=90 and f'_c=120 MPa, the axial capacity of column C-120-497-90-0-3, C-120-536-90-0-3, C-120-622-90-0-3 and C-120-707-90-0-3 are increased by 6%, 12%, 14% and 17% than column C-30-448-90-0-3 with the increment of proof steel strength 11%, 20%, 39% and 58% respectively. On the other hand, code (AISC-LRFD 2010) predicted capacity increment were 2%, 4%,7% and 10%, respectively.

Similarly, from Table 6.3d where D/t=30 and f'_c=30 MPa, the axial capacity of column C-30-497-30-0-3, C-30-536-30-0-3, C-30-6225-30-0-3 and C-30-707-30-0-3 are increased by 8%, 14%, 27% and 41% than column C-30-448-30-0-3, with the increment of proof steel strength 11%, 20%, 39% and 58% respectively. On the other hand, code (AISC-LRFD 2010) predicted capacity increment were 8%, 14%,28% and 42%, respectively.

Again when D/t=30 and f'_c=120 MPa, the axial capacity of column C-30-497-30-0-3, C-30-536-30-0-3, C-30-6225-30-0-3 and C-30-707-30-0-3 are increased by 4%, 7%, 12% and 19% than column C-30-448-30-0-3, with the increment of proof steel strength 11%, 20%, 39% and 58% respectively. On the other hand, code (AISC-LRFD 2010) predicted capacity increment were 4%, 7%,15% and 22%, respectively.

Axial capacity of column with the increment of steel strength is depends on the concrete strength and steel wall thickness (D/t). Concrete strength is more sensitive for higher grade of steel. The code (AISC-LRFD 2010) predicted capacity behaviour was also same with the numerical bahaviour.

6.5.3 Modes of Failure

The failures in the columns in set-21 occurred by crushing of concrete followed by yielding of steel. The crushing of concrete (CC) started near the middle of the columns. The deformed shape of column C_45_448_90_0_3 with stress contour at failure of concrete was captured as shown in Figure 6.5a and 6.5b, similarly the contour at failure of stainless steel was captured as shown in Figure 6.5c and overall failure deformed shape shown as Figure 6.5d. From the all figures it is observed that Von Mises stress failure (yield) of the structural steel and concrete of column was started near the middle of the columns.

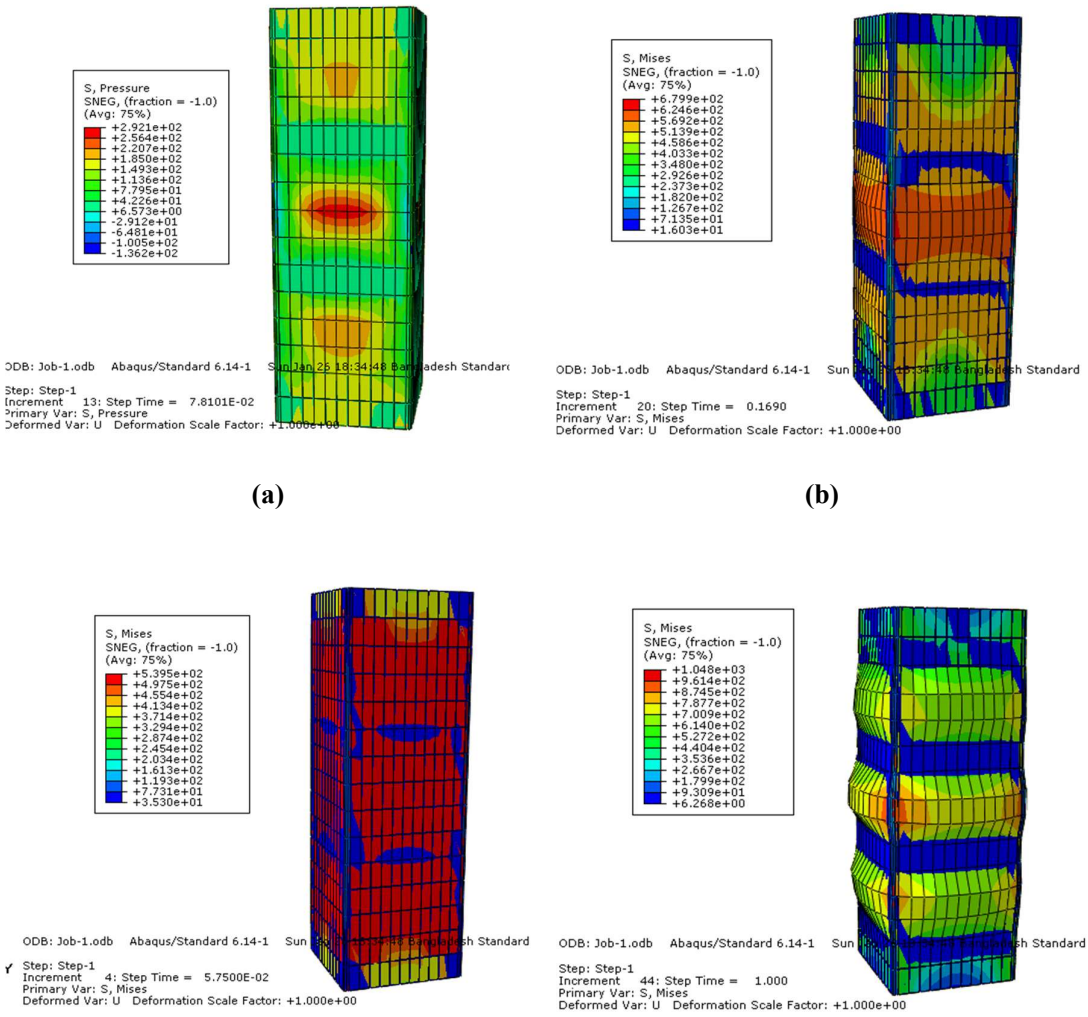

Figure 6.5: Modes of failure, (a) & (b) Stress contour of concrete at failure; (c) Stress contour of steel at failure; (d) Overall failure.

6.6 Effect of Column Depth to Thickness Ratio, (D/t)

The column depth to thickness (D/t) ratio is defined as the ratio of the depth/width of Column (D), to the stainless-steel thin wall thickness (t) of the column cross-section. Column depth to thickness (D/t) ratio has a great influence for load carrying capacity. In this study, fourty columns were simulated to observe the effect (D/t) ratio. Four different depth to thickness (D/t) ratio 30 (t = 15 mm), 50 (t = 9 mm), 75 (t = 6 mm) and 90 (t = 5 mm) were employed with ten sets (set-45 to 54) in the parametric study as shown in Table

6.3. Concrete compressive strength for set-45, 46, 47, 48, 49 and 50 were 30 MPa, 45 MPa, 60 MPa, 80 MPa, 100 MPa and 120 MPa, respectively with steel strength 448 MPa. For set-51 and 52 concrete compressive strength were 60 & 80 MPa with steel strength 536 MPa and for set 53 and 54 concrete compressive strength were 100 & 120 MPa with steel strength 707 MPa. This study was done only for concentric load with constant L/D (L=1350 mm) ratios.

Table 6.3: Effect of Column Depth to Thickness Ratio (D/t)

Set	Specimen designation	Column Properties				Axial Capacity (kN)		$\frac{P_{AISC}}{P_{FE}}$
		D/t	L/D	f_y (MPa)	f'_c (MPa)	P_{FE}	P_{AISC}	
Set-45	C-30-448-30-0-3	90	3	448	30	9160	8924	0.974
	C-30-448-50-0-3	75	3	448	30	10176	9665	0.950
	C-30-448-75-0-3	50	3	448	30	12993	11871	0.914
	C-30-448-90-0-3	30	3	448	30	18022	16191	0.898
Set-46	C-45-448-30-0-3	90	3	448	45	11917	11392	0.956
	C-45-448-50-0-3	75	3	448	45	13056	12112	0.928
	C-45-448-75-0-3	50	3	448	45	15800	14250	0.902
	C-45-448-90-0-3	30	3	448	45	20508	18440	0.899
Set-47	C-60-448-30-0-3	90	3	448	60	14935	13860	0.928
	C-60-448-50-0-3	75	3	448	60	15952	14557	0.913
	C-60-448-75-0-3	50	3	448	60	18587	16630	0.895
	C-60-448-90-0-3	30	3	448	60	22834	20689	0.906
Set-48	C-80-448-30-0-3	90	3	448	80	19056	17115	0.898
	C-80-448-50-0-3	75	3	448	80	19857	17819	0.935
	C-80-448-75-0-3	50	3	448	80	22255	19802	0.890
	C-80-448-90-0-3	30	3	448	80	26335	23688	0.899

Table 6.3: Effect of Column Depth to Thickness Ratio (D/t)

Set	Specimen designation	Column Properties				Axial Capacity (kN)		$\frac{P_{AISC}}{P_{FE}}$
		D/t	L/D	f_y (MPa)	f'_c (MPa)	P_{FE}	P_{AISC}	
Set-49	C-100-448-30-0-3	90	3	448	100	23036	20433	0.887
	C-100-448-50-0-3	75	3	448	100	23177	21080	0.910
	C-100-448-75-0-3	50	3	448	100	26066	22975	0.882
	C-100-448-90-0-3	30	3	448	100	29866	26686	0.894
Set-50	C-120-448-90-0-3	90	3	448	120	26073	23731	0.910
	C-120-448-75-0-3	75	3	448	120	26799	24341	0.908
	C-120-448-50-0-3	50	3	448	120	27851	26148	0.939
	C-120-448-30-0-3	30	3	448	120	33501	29686	0.886
Set-51	C-60-536-30-0-3	30	3	536	60	15694	14644	0.933
	C-60-536-50-0-3	50	3	536	60	16748	15496	0.925
	C-60-536-75-0-3	75	3	536	60	20037	18027	0.900
	C-60-536-90-0-3	90	3	536	60	25489	22986	0.902
Set-52	C-80-536-30-0-3	30	3	536	80	19295	17935	0.930
	C-80-536-50-0-3	50	3	536	80	20651	18757	0.908
	C-80-536-75-0-3	75	3	536	80	23745	21200	0.893
	C-80-536-90-0-3	90	3	536	80	28616	25985	0.908
Set-53	C-100-707-30-0-3	30	3	707	100	24601	22748	0.925
	C-100-707-50-0-3	50	3	707	100	25298	23841	0.942
	C-100-707-75-0-3	75	3	707	100	29687	27087	0.912
	C-100-707-90-0-3	90	3	707	100	36670	33447	0.912
Set-54	C-120-707-30-0-3	30	3	707	120	28738	26040	0.906
	C-120-707-50-0-3	50	3	707	120	29448	27402	0.931
	C-120-707-75-0-3	75	3	707	120	33668	30260	0.899
	C-120-707-90-0-3	90	3	707	120	39849	36440	0.914

6.6.1 Load versus Average Axial Deformation Response

Figures 6.6a, 6.6b, 6.6c, 6.6d, 6.6e, 6.6f, 6.6g and f 6.6h represents the effects depth to thickness ratio of structural steel on the axial load versus average axial deformation responses for column Set-45, set-46, set-47, set-48, set-49,Set-50, set-53 and set-54 respectively. It is apparent from the figures, the ultimate capacity of CFSST columns decreases with the increasing of depth to thickness ratio of structural steel.

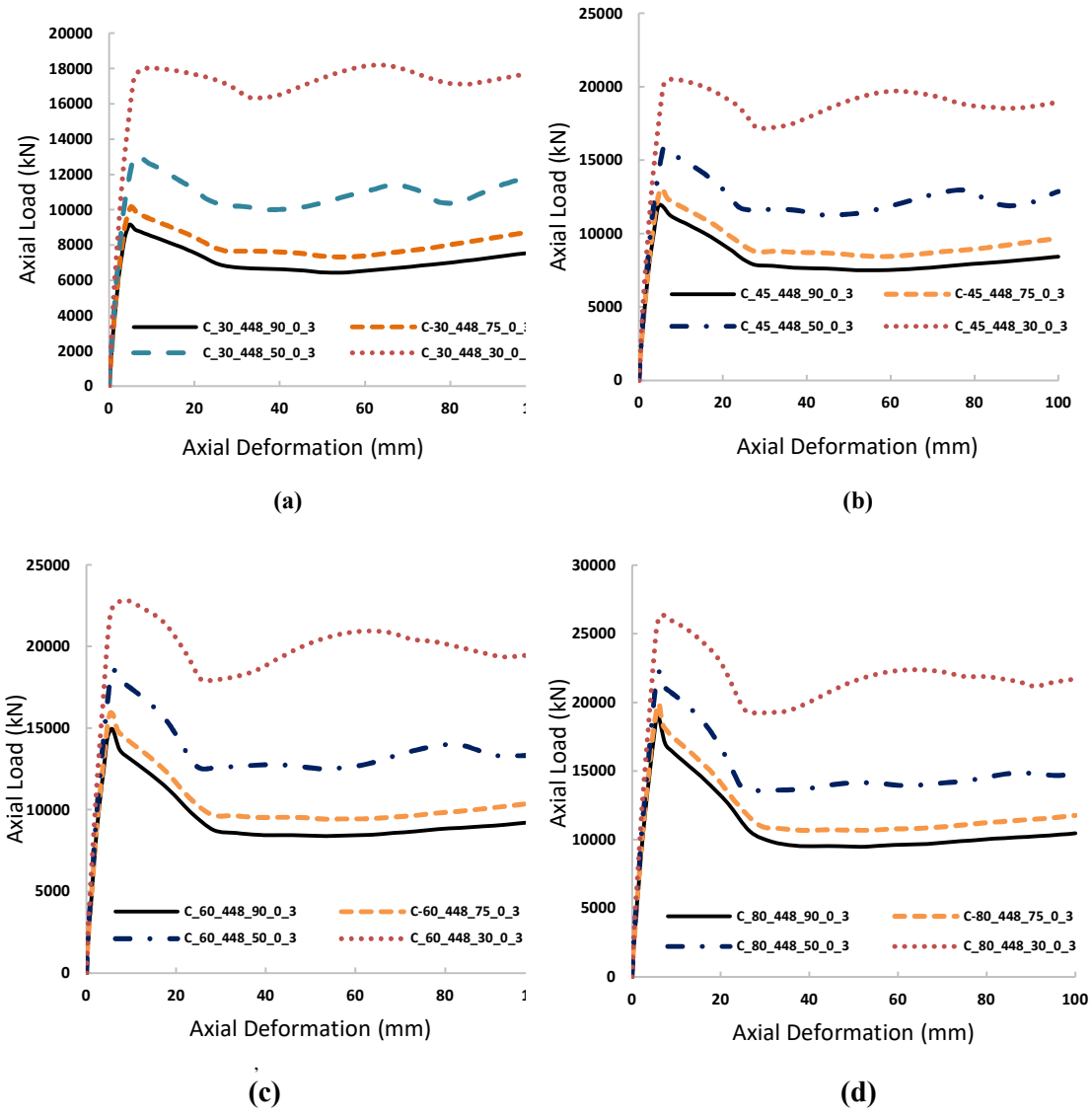

Figure 6.6: Effect of column depth to thickness ratio (D/t), (a) axial load vs axial deformation curve (Set-45); (b) axial load vs axial deformation curve (Set-46); (c) axial load vs axial deformation curve (Set-47); (d) axial load vs axial deformation curve (Set-48).

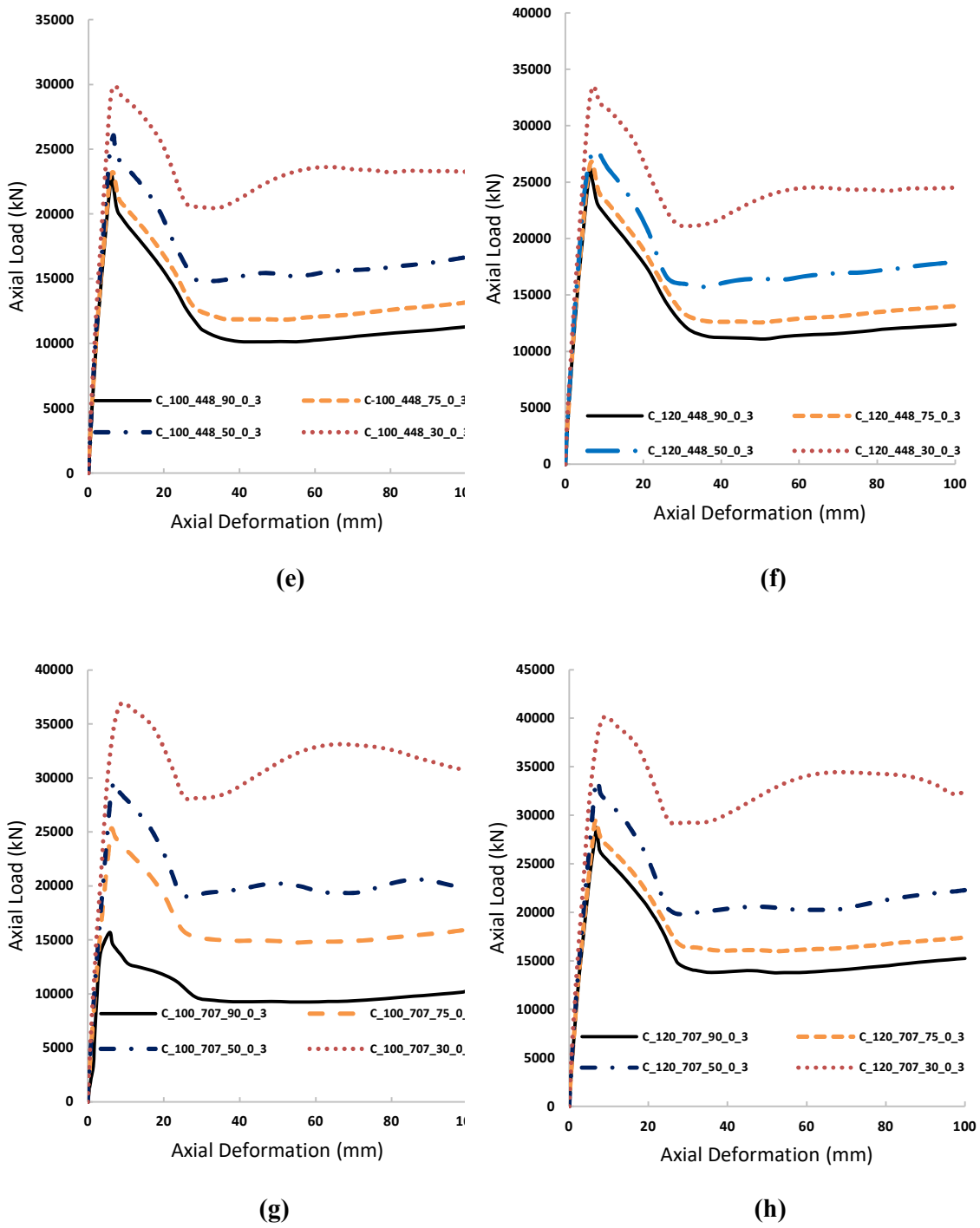

Figure 6.6: Effect of column depth to thickness ratio (D/t), (e) load vs axial deformation curve (Set-49); (f) load vs axial deformation curve (Set-50); (g) load vs axial deformation curve (Set-51); (h) load vs axial deformation curve (Set-52).

6.6.2 Comparison of Peak Load

It is observed from Table 6.3 that the axial capacity of columns set-45 i.e. C-30-448-75-0-3, C-30-448-50-0-3 and C-30-448-30-0-3 are increased by 11%, 41% and 96% than column C-30-448-90-0-3 with the increment of steel thickness from 5 mm (D/t = 90) to 6 mm (D/t = 75), 9 mm (D/t = 50) and 15 mm (D/t = 30) respectively. On the other hand, codes (AISC-LRFD 2010) predicted capacity increment were 8%, 33% and 81%, respectively.

Similarly, axial capacity of column set-46, i.e. C-45-448-75-0-3, C-45-448-50-0-3 and C-45-448-30-0-3 are increased by 6%, 25% and 62% than column C-45-448-90-0-3, column set-50 i.e. C-120-448-75-0-3, C-120-448-50-0-3 and C-120-448-90-0-3 are increased by 3%, 7% and 29% than column C-120-448-90-0-3 respectively. On the other hand, codes (AISC-LRFD 2010) predicted capacity increment were 6%, 25%, 62% and 3%, 10%, 26% respectively. In fact, percentage of incremental rate of column capacity is decreasing with the increment of D/t ratio.

Effect of stainless-steel wall thickness 't' is significant lower grade of concrete and steel. On the other hand, 't' is less significant for higher grade of concrete and steel strength. The code (AISC-LRFD 2010) predicted capacity was also same with the numerical.

6.6.3 Modes of Failure

The failures in the columns in set-45 occurred by crushing of concrete followed by yielding of steel. The crushing of concrete (CC) started near the middle of the columns. The deformed shape of column C_30_448_90_0_3 with stress contour at failure of concrete was captured as shown in Figure 6.5a and 6.5b, similarly the contour at failure of stainless steel was captured as shown in Figure 6.5c and overall failure deformed shape shown as Figure 6.5d. From the all figures it is observed that Von Mises stress failure (yield) of the structural steel and concrete of column was started near the middle of the columns.

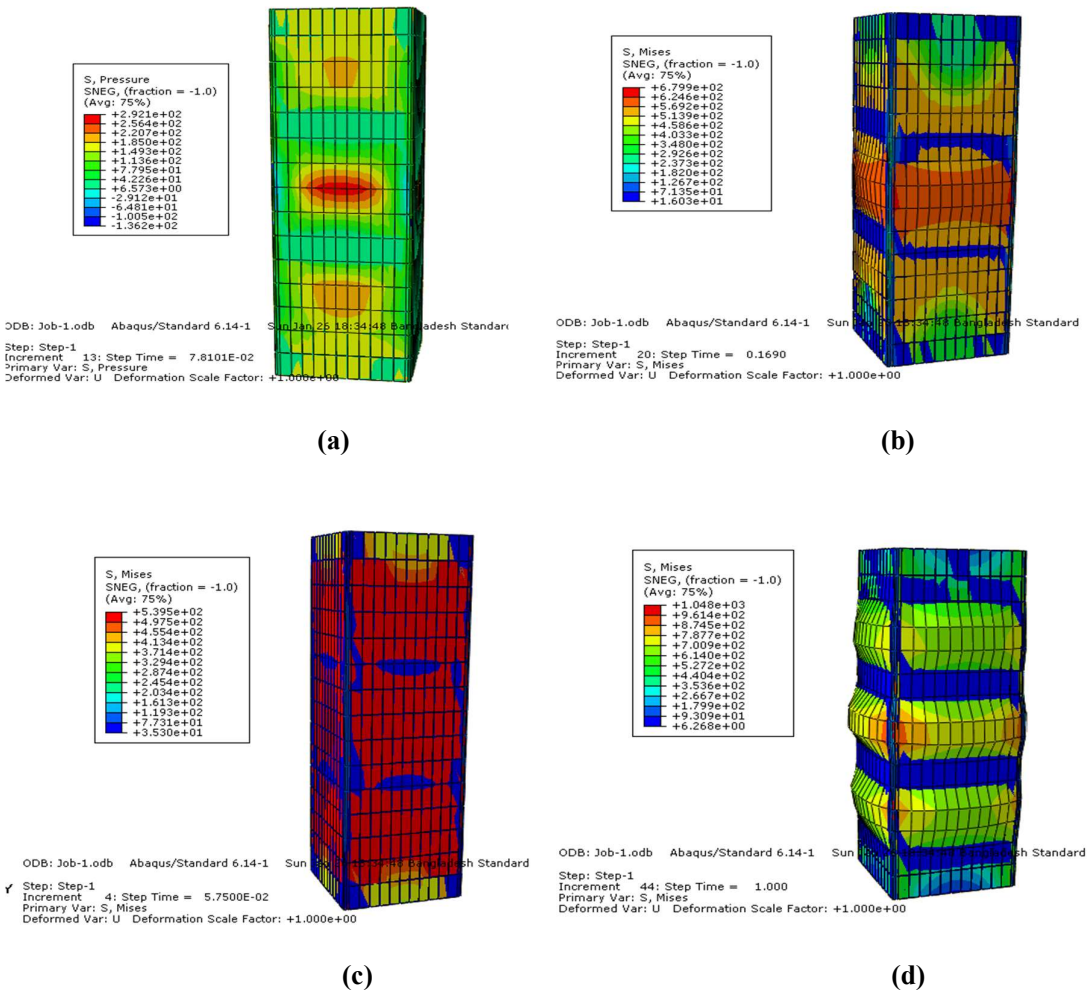

Figure 6.7: Modes of failure, (a) & (b) Stress contour of concrete at failure; (c) Stress contour of steel at failure; (d) Overall failure.

6.7 Effect of Load Eccentricity Ratio, (e/D)

The influence of load eccentricity ratio of CFSST columns under bending induced by eccentrically applied axial load is greatly affected by the initial load eccentricity ratio. In this study, thirty columns were simulated to observe the effect (e/D) ratio. Four different eccentricity (e/D) ratio 0.05 (e = 22.5 mm), 0.10 (e = 45 mm), 0.15 (e = 67.5 mm) and 0.2 (e = 90 mm) were employed with six sets (set-55 to 60) in the parametric study as shown in Table 6.4. Concrete compressive strength was used 30 MPa for sets 55, 57, 59 with steel strength 448, 497, 536 MPa respectively and Concrete strength was taken 45 MPa for sets-56, 58, 60 with steel strength 448, 497, 436 MPa respectively.

Table 6.4: Effect of Load Eccentricity Ratio (e/D)

Set	Specimen designation	Column Properties					Axial Capacity (kN)		$\frac{P_{AISC}}{P_{FE}}$
		e/D	D/t	L/D	f_y (MPa)	f'_c (MPa)	P_{FE}	P_{AISC}	
	C-30-448-90-0-3	0	90	3	448	30	9220	8924	0.968
Set-55	C-30-448-90-22.5-3	0.05	90	3	448	30	8285	7680	0.927
	C-30-448-90-45-3	0.10	90	3	448	30	7336	6668	0.909
	C-30-448-90-67.5-3	0.15	90	3	448	30	6702	6139	0.916
	C-30-448-90-90-3	0.20	90	3	448	30	5917	5491	0.928
	C-45-448-90-0-3	0	90	3	448	45	11917	11392	0.956
Set-56	C-45-448-90-22.5-3	0.05	90	3	448	45	10519	10077	0.958
	C-45-448-90-45-3	0.10	90	3	448	45	9363	8811	0.941
	C-45-448-90-67.5-3	0.15	90	3	448	45	8376	7865	0.939
	C-45-448-90-90-3	0.20	90	3	448	45	7550	7006	0.928
	C-30-497-90-0-3	0	90	3	497	30	9476	9365	0.988
Set-57	C-30-497-90-22.5-3	0.05	90	3	497	30	8434	8164	0.968
	C-30-497-90-45-3	0.10	90	3	497	30	7578	7222	0.953
	C-30-497-90-67.5-3	0.15	90	3	497	30	6820	6499	0.953
	C-30-497-90-90-3	0.20	90	3	497	30	6275	5892	0.939
	C-45-497-90-0-3	0	90	3	497	45	12103	11829	0.977
Set-58	C-45-497-90-22.5-3	0.05	90	3	497	45	10891	10444	0.959
	C-45-497-90-45-3	0.10	90	3	497	45	9553	9008	0.943
	C-45-497-90-67.5-3	0.15	90	3	497	45	8741	8286	0.948
	C-45-497-90-90-3	0.20	90	3	497	45	7786	7202	0.925
Set-59	C-30-536-75-0-3	0	75	3	536	30	10860	10604	0.976
	C-30-536-75-22.5-3	0.05	75	3	536	30	9729	9311	0.957
	C-30-536-75-45-3	0.10	75	3	536	30	8650	8226	0.951
	C-30-536-75-67.5-3	0.15	75	3	536	30	7853	7343	0.935
	C-30-536-75-90-3	0.20	75	3	536	30	7144	6915	0.968

Table 6.4: Effect of Load Eccentricity Ratio (e/D)

Set	Specimen designation	Column Properties					Axial Capacity (kN)		$\frac{P_{AISC}}{P_{FE}}$
		e/D	D/t	L/D	f_y (MPa)	f'_c (MPa)	P_{FE}	P_{AISC}	
Set-60	C-45-536-75-0-3	0	75	3	536	45	13742	13050	0.950
	C-45-536-75-22.5-3	0.05	75	3	536	45	12102	11388	0.941
	C-45-536-75-45-3	0.10	75	3	536	45	10751	10095	0.939
	C-45-536-75-67.5-3	0.15	75	3	536	45	9633	8939	0.928
	C-45-536-75-90-3	0.20	75	3	536	45	8846	8413	0.951

6.7.1 Load versus Average Axial Deformation Response

Figures 6.8a, 6.8b, 6.8c, 6.8d, 6.8e and 6.8f shows the effects of eccentricity (e/D) ratio on the axial load versus axial deformation responses for Set-55, 56, 57, 58, 59 and 60 columns respectively. It is apparent from the figures that as the eccentricity (e/D) ratio is increased, the stiffness and the ultimate capacity of CFSST column decreases. The residual strength after failure and ductility of the columns were also observed to decrease significantly with the increase in the eccentricity (e/D) ratio.

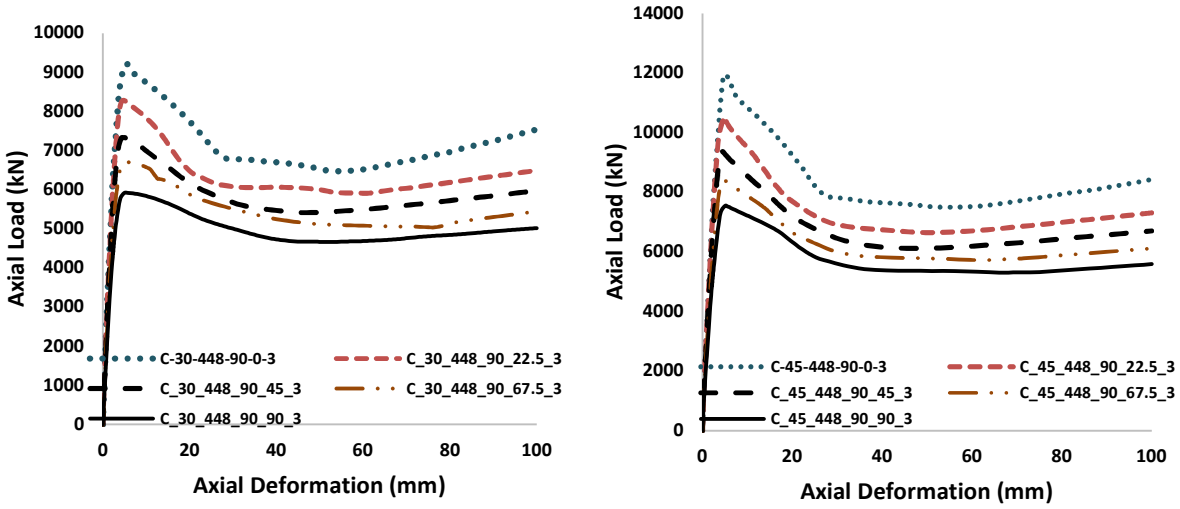

(a) **(b)**

Figure 6.8: Effect of (e/D) ratio on axial load vs axial deformation, (a) axial load vs axial deformation curve (Set-55); (b) axial load vs axial deformation curve (Set-56).

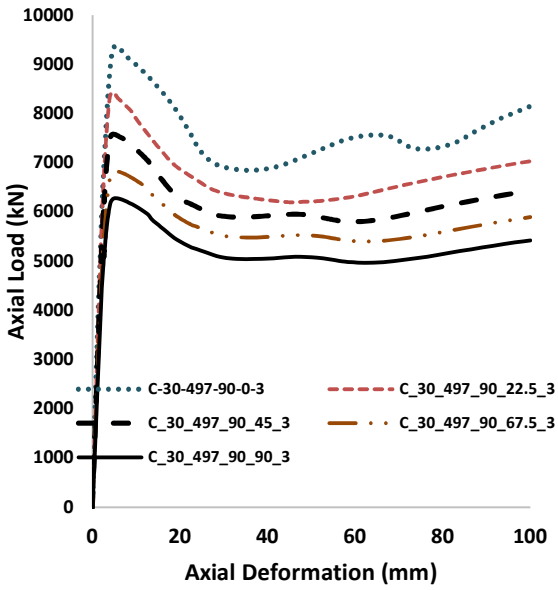

(c)

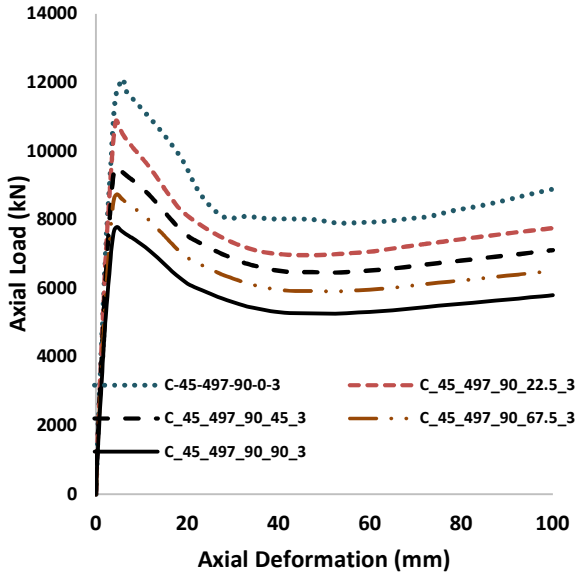

(d)

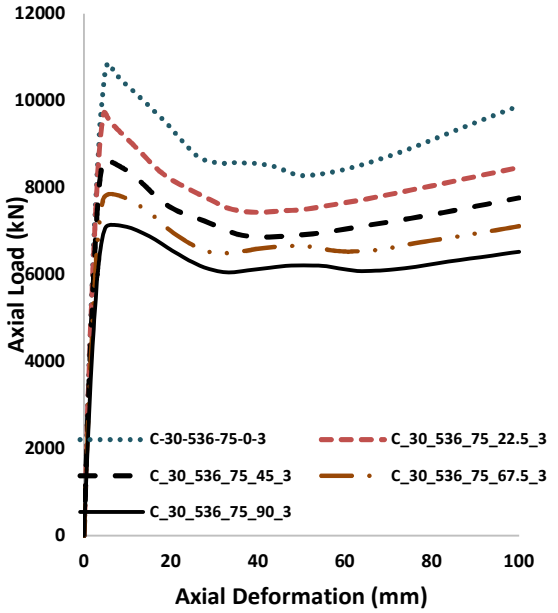

(e)

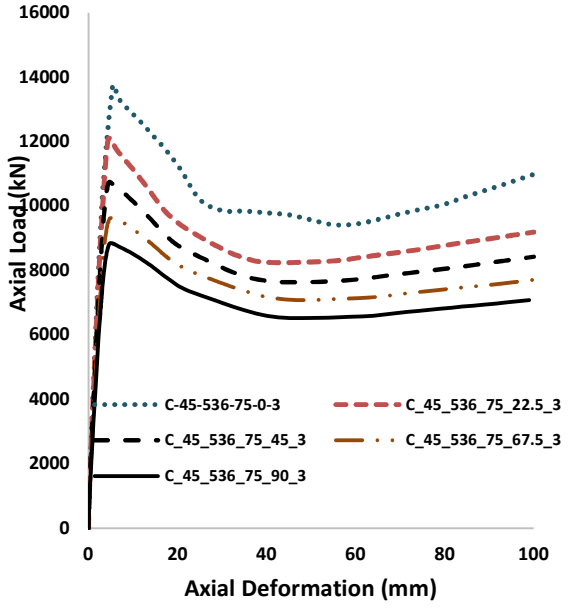

(f)

Figure 6.8: Effect of (e/D) ratio on axial load vs axial deformation, (c) axial load vs axial deformation curve (Set-57); (d) axial load vs axial deformation curve (Set-58); (e) axial load vs axial deformation curve (Set-59); (f) axial load vs axial deformation curve (Set-60).

6.7.2 Comparison of Peak Load

It is observed from Table 6.4 that the axial capacity of column C-30-448-90-0-3, decreased by 11%, 20%, 27% and 36% with the increment of eccentricity (e/D) ratio from 0 to 0.05, 0.10, 0.15 and 0.20, respectively and axial capacity for column C-45-448-90-0-3 decreased by 12%, 21%, 30% and 37% with the increment of eccentricity (e/D) ratio from 0 to 0.05, 0.10, 0.15 and 0.20, respectively. On the other hand, code (AISC-LRFD 2010) predicted capacity decrement were 14%, 26% , 32%, 38% and 12%, 23%, 31%, 39% respectively.

Similarly, axial capacity of columns C-30-497-90-0-3 and C-45-497-90-0-3 are decreased by 11%, 20%, 28%, 34% and 10%, 21%, 28% and 36%, with the increment of eccentricity (e/D) ratio from 0 to 0.05, 0.10, 0.15 and 0.20, respectively, and Columns capacity of C-30-536-75-0-3 and C-45-536-75-0-3 are decreased by 10%, 20%, 28%, 34% and 12%, 22%, 29% and 36%, with the increment of eccentricity (e/D) ratio from 0 to 0.05, 0.10, 0.15 and 0.20, respectively.

Axial capacity of column decrement rate was higher with higher grade concrete. The code (AISC-LRFD 2010) predicted capacity behaviour was almost same in spite of increasing the concrete grade.

6.7.3 Modes of Failure

The failures in the columns occurred by crushing of concrete followed by yielding of steel. The crushing of concrete (CC) occurred at the compression side of the columns near the middle zone. The deformed shape with stress contour at failure of concrete was captured as shown in Figure 6.9a and 6.9b of column C-30-448-90-45-3. Similarly, the contour at failure of stainless steel was captured as shown in Figure 6.9c and overall failure deformed shape shown as Figure 6.9d. From the all figures it is observed that Von Mises stress failure (yield) of the structural steel and concrete of column was started near the middle of the columns.

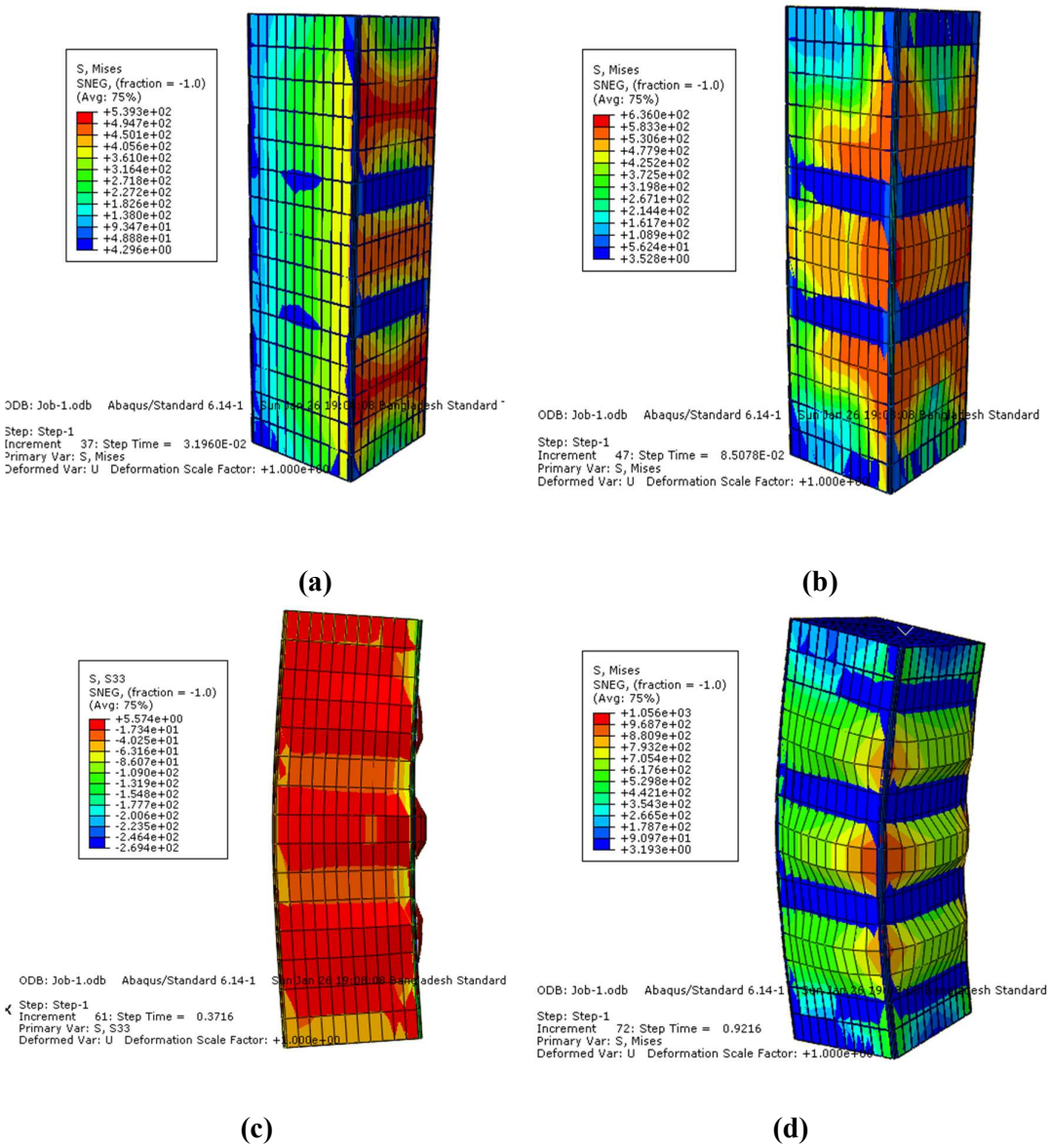

Figure 6.9: Modes of failure, (a) & (b) Stress contour of concrete at failure; (c) Stress contour of steel at failure; (d) Stress contour of overall failure.

6.8 Effect of Column Slenderness Ratio, (L/D)

The column slenderness ratio is defined as the ratio of the length (L), to the depth of the column cross-section (D). The global stability of the column is controlled by the slenderness (L/D) ratio. Six different slenderness ratios 3 (L=1350 mm), 5 (L=2250 mm), 7 (3150 mm) 10 (L=4500 mm), 15 (L=6750 mm) and 20 (L=9000 mm) were employed in the parametric

study (as shown in Table 6.5) to cover the range of short, intermediate and long columns. Stainless steel strength was taken 448, 497 and 536 MPa, for each steel strength, 30 and 45 MPa concrete compressive strength was used. For this slenderness effect study, D/t ratio was used 75 and eccentricity was taken 10 mm for all the sets set-61, 62, 63, 64, 65 and 66. That is the D/t and eccentricity was constant for all models where the steel strength (448, 497,536 MPa) and concrete (30, 45 MPa) strength was variable.

Table 6:5 Effect of Column Slenderness Ratio (L/D)

Set	Specimen designation	Column Properties					Axial Capacity (kN)		$\frac{P_{AISC}}{P_{FE}}$
		e/D	D/t	L/D	f_y (MPa)	f'_c (MPa)	P_{FE}	P_{AISC}	
	C-30-448-75-0-3	0.022	75	3	448	30	9753	9236	0.947
Set	C-30-448-75-0-5	0.022	75	5	448	30	9698	9106	0.939
-61	C-30-448-75-0-7	0.022	75	7	448	30	9323	8717	0.935
	C-30-448-75-0-10	0.022	75	10	448	30	8587	8098	0.943
	C-30-448-75-0-15	0.022	75	15	448	30	7807	7424	0.951
	C-30-448-75-0-20	0.022	75	20	448	30	6623	6332	0.956
	C-45-448-75-0-3	0.022	75	3	448	45	12331	11480	0.931
Set	C-45-448-75-0-5	0.022	75	5	448	45	12269	11226	0.915
-62	C-45-448-75-0-7	0.022	75	7	448	45	11875	10937	0.921
	C-45-448-75-0-10	0.022	75	10	448	45	11559	10553	0.913
	C-45-448-75-0-15	0.022	75	15	448	45	9749	9076	0.931
	C-45-448-75-0-20	0.022	75	20	448	45	7732	7160	0.926
	C-30-497-75-0-3	0.022	75	3	497	30	10111	9292	0.919
Set	C-30-497-75-0-5	0.022	75	5	497	30	9954	9188	0.923
-63	C-30-497-75-0-7	0.022	75	7	497	30	9651	8985	0.931
	C-30-497-75-0-10	0.022	75	10	497	30	8899	8240	0.926
	C-30-497-75-0-15	0.022	75	15	497	30	8287	7607	0.918
	C-30-497-75-0-20	0.022	75	20	497	30	7344	6712	0.914

Table 6:5 Effect of Column Slenderness Ratio (L/D)

Set	Specimen designation	Column Properties					Axial Capacity (kN)		$\frac{P_{AISC}}{P_{FE}}$
		e/D	D/t	L/D	f_y (MPa)	f'_c (MPa)	P_{FE}	P_{AISC}	
Set-64	C-45-497-75-0-3	0.022	75	3	497	45	12742	11761	0.923
	C-45-497-75-0-5	0.022	75	5	497	45	12590	11822	0.939
	C-45-497-75-0-7	0.022	75	7	497	45	12285	11486	0.935
	C-45-497-75-0-10	0.022	75	10	497	45	11080	10227	0.923
	C-45-497-75-0-15	0.022	75	15	497	45	9890	9109	0.921
	C-45-497-75-0-20	0.022	75	20	497	45	8375	7672	0.916
Set-65	C-30-536-75-0-3	0.022	75	3	536	30	10421	9764	0.937
	C-30-536-75-0-5	0.022	75	5	536	30	10337	9427	0.912
	C-30-536-75-0-7	0.022	75	7	536	30	9622	8862	0.921
	C-30-536-75-0-10	0.022	75	10	536	30	9198	8425	0.916
	C-30-536-75-0-15	0.022	75	15	536	30	7979	7349	0.921
	C-30-536-75-0-20	0.022	75	20	536	30	6757	6230	0.922
Set-66	C-45-536-75-0-3	0.022	75	3	536	45	13109	12086	0.922
	C-45-536-75-0-5	0.022	75	5	536	45	13045	11975	0.918
	C-45-536-75-0-7	0.022	75	7	536	45	11957	11132	0.931
	C-45-536-75-0-10	0.022	75	10	536	45	11461	10590	0.924
	C-45-536-75-0-15	0.022	75	15	536	45	9971	9163	0.919
	C-45-536-75-0-20	0.022	75	20	536	45	8395	7707	0.918

6.8.1 Load versus Average Axial Deformation Responses

Figures 6.10a, 6.10b, 6.10c, 6.10d, 6.10e and 6.10f shows the effects of columns slenderness (L/D) ratio on the axial load versus average axial deformation responses for Set-61, Set-62, Set-63, Set-64, Set-65 and Set-66 respectively. It is apparent from the figures that as the slenderness (L/D) ratio is increased the stiffness and the ultimate capacity of CFSST column decreases. The residual strength after failure and ductility of the columns were also observed to decrease significantly with the increase in the slenderness (L/D) ratio. This behaviour is observed for columns of Set-61, Set-62, Set-63, Set-64, Set-65 and Set-66.

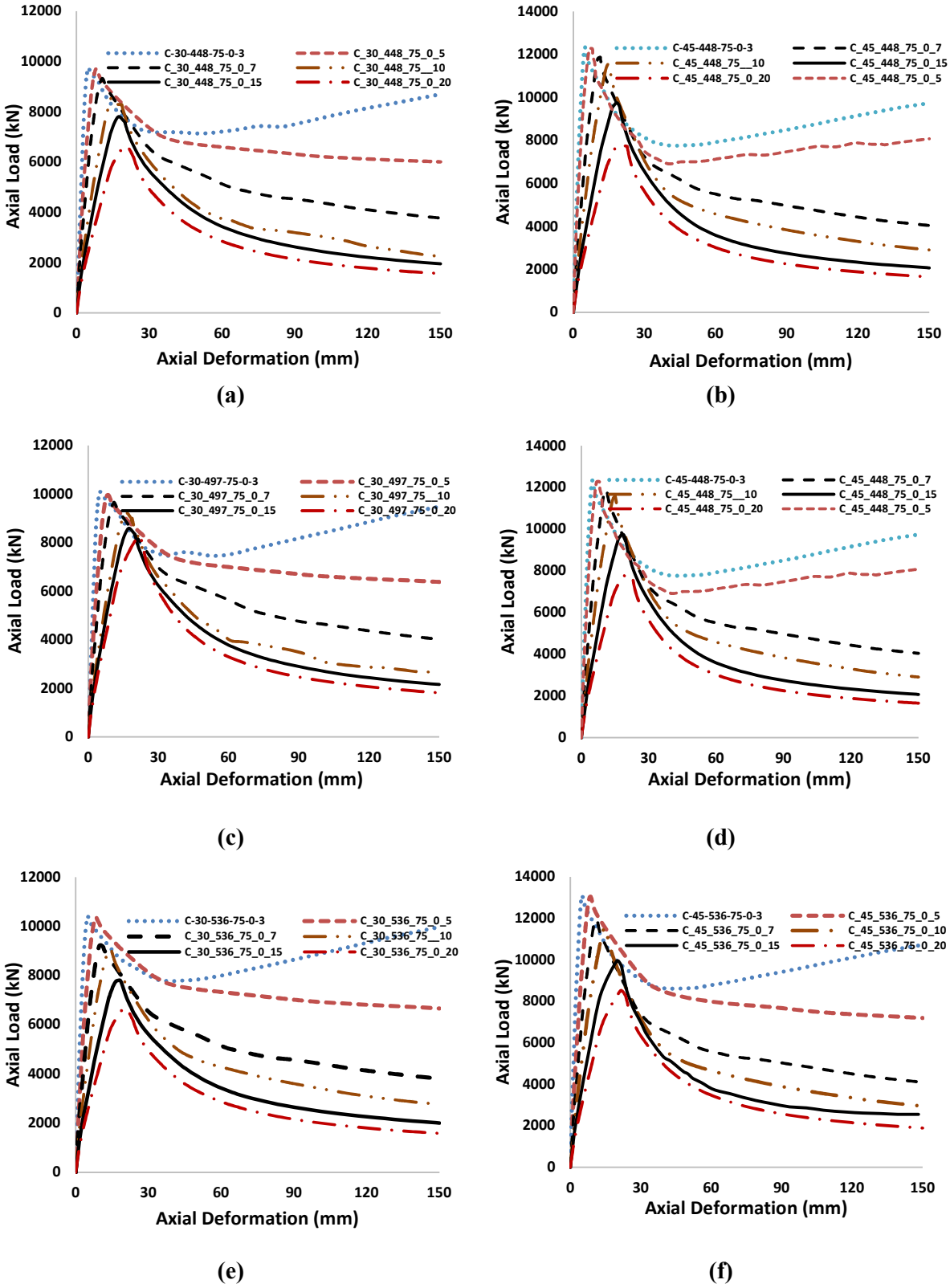

Figure 6.10: Effect of L/D ratio on axial load vs axial deformation curve, (a) axial load vs axial deformation curve (Set-61); (b) axial load vs axial deformation curve (Set-62); (c) axial load vs axial deformation curve (Set-63); (d) axial load vs axial deformation curve (Set-64); (e) axial load vs axial deformation curve (Set-65); (f) axial load vs axial deformation curve (Set-66);.

6.8.2 Comparison of Peak Load

It is observed from Table 6.5 that the axial capacity of column C-30-448-75-0-3 and decreased by 2%, 4%, 8%, 20% and 37% with the increment of slenderness (L/D) ratio from 3 to 5, 7, 10, 15, and 20, respectively and axial capacity for column C-45-448-75-0-3 decreased by 1%, 4%, 6%, 21% and 37% with the increment of slenderness (L/D) ratio from 3 to 5, 7, 10, 15, and 20, respectively. On the other hand, code (AISC-LRFD 2010) predicted capacity for C-30-448-75-0-3 and C-45-448-75-0-3 decrement were 1%, 6%, 12%, 20%, 31 % and 2%, 5%, 8%, 21%, 38% respectively.

Similarly, axial capacity of columns C-30-497-75-0-3 and C-45-497-75-0-3 are decreased by 1%, 5%, 12%, 21%, 30% and 2%, 4% 13%, 22%, 34% with the increment of slenderness (L/D) ratio from 3 to 5, 7, 10, 15, and 20, respectively and Columns capacity of C-30-536-75-0-3 and C-45-536-75-0-3 are decreased by 1%, 7% 12%, 23%, 35% and 1%, 9%, 13%, 24%, 36%, with the increment of slenderness (L/D) ratio from 3 to 5, 7, 10, 15, and 20, respectively.

Axial capacity of column decrement rate was higher with higher grade concrete. The code (AISC-LRFD 2010) predicted capacity behaviour was almost same in spite of increasing the concrete grade.

6.8.3 Modes of Failure

The failure in the columns was attained by crushing of concrete followed by yielding of steel. The crushing of concrete occurred at the compression side of the columns. Figure 6.11a shows the deformed shape along with stress contour at failure. The failures of the columns were attained mainly due to crushing of concrete at the compression side of the column. The data obtained from FE analysis showed that the structural steel reached its yield stress and flexural buckling failure mode was governed by the concrete elements at the maximum stressed fibers. Figure 6.11b shows the deformed shape of structural steel at failure.

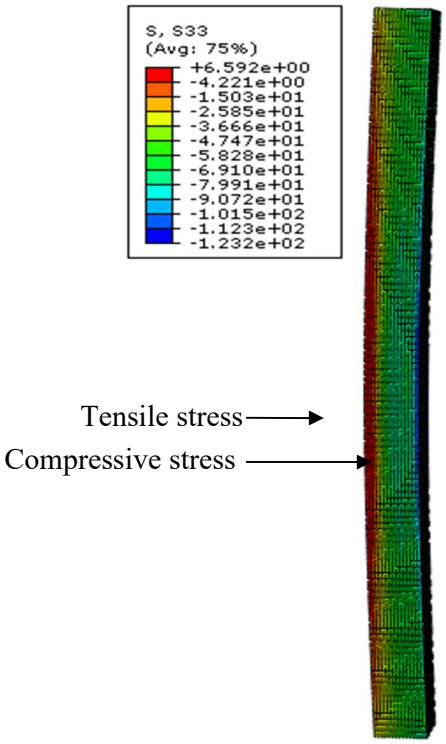

Figure 6.11: Stress contour of concrete at failure.

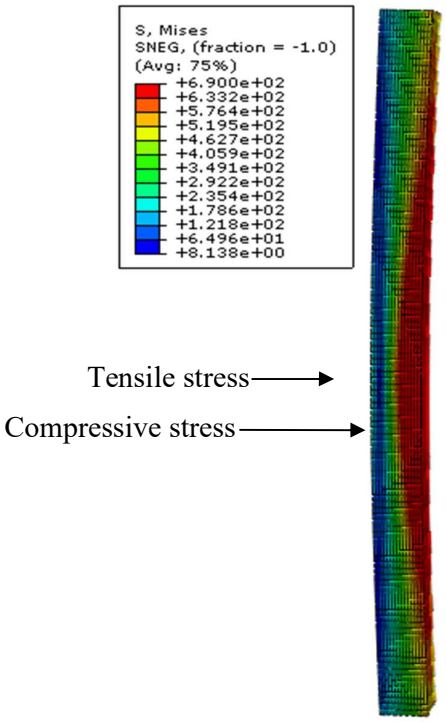

Figure 6.12: Stress contour of steel at failure.

6.9 Summery of Parametric Study

Parametric study was carried out varying concrete compressive strength, steel strength, depth to thickness ratio (D/t), slenderness ratio (L/D) and eccentricity ratio (e/D). Compressive strength were 30 MPa, 45 MPa, 60 MPa, 80 MPa, 100 MPa and 120 MPa with steel strength 448 MPa, 497 MPa, 536 MPa, 622 MPa and 707 MPa. The depth-to-thickness (D/t) ratios of these columns were 90, 75, 50 and 30. The load carrying capacity of the CFSST columns were found to increase with a decrease of depth-to-thickness (D/t) ratio. Following figures represents the capacity of individual CFSST column varying different parameters.

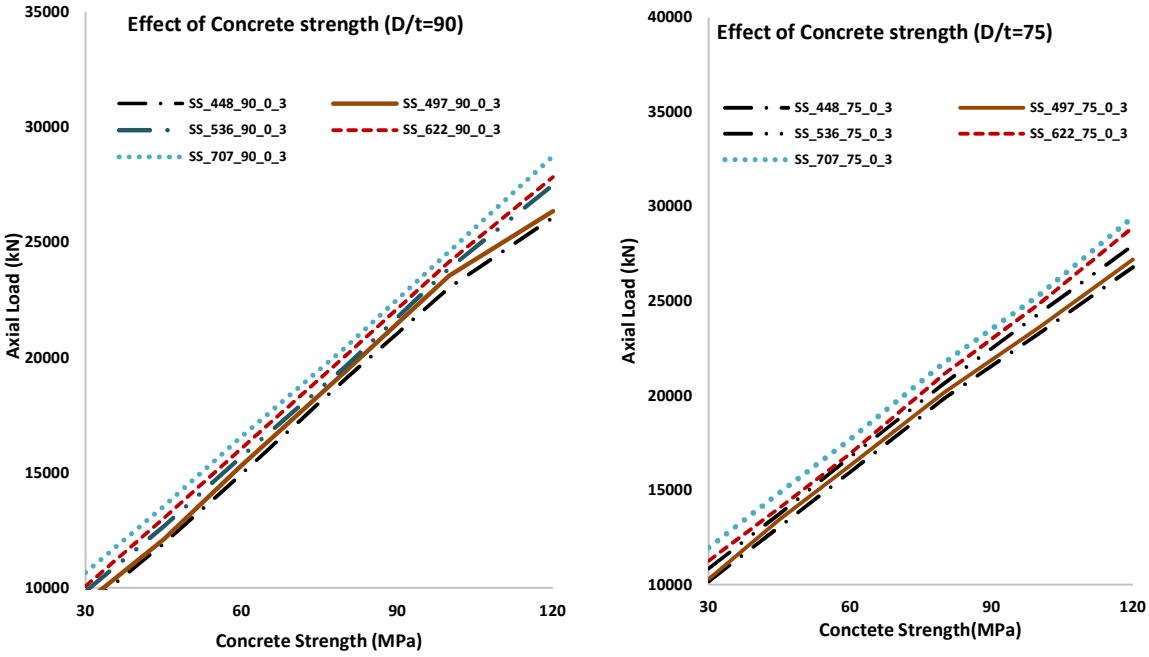

Figure 6.13: Effects of concrete strength with steel strength for different D/t, (a) D/t = 90; (b) D/t = 75;

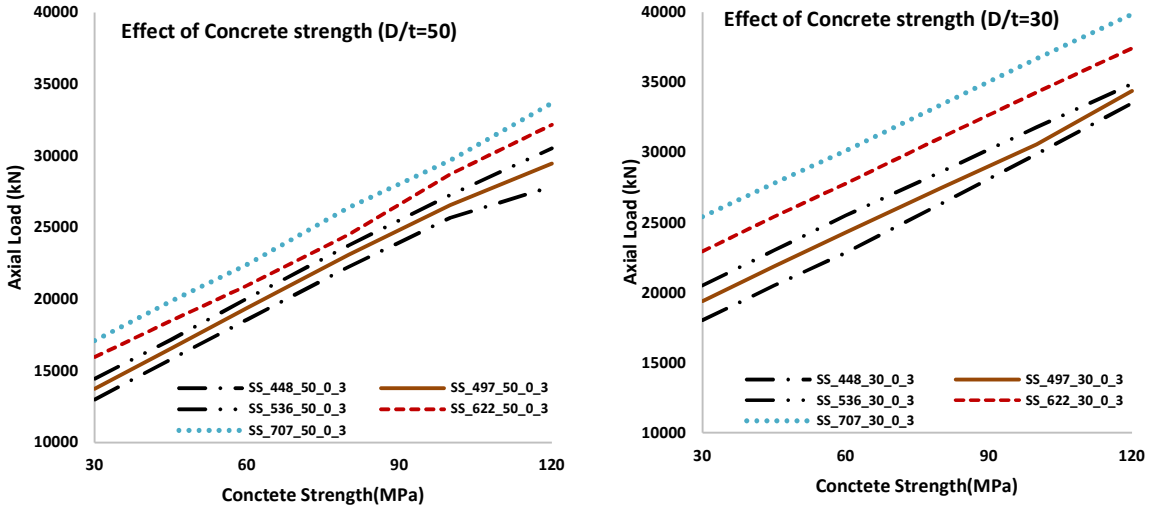

(c) (d)

Figure 6.13: Effects of concrete strength with steel strength for different D/t, (C) D/t = 50; (d) D/t = 30.

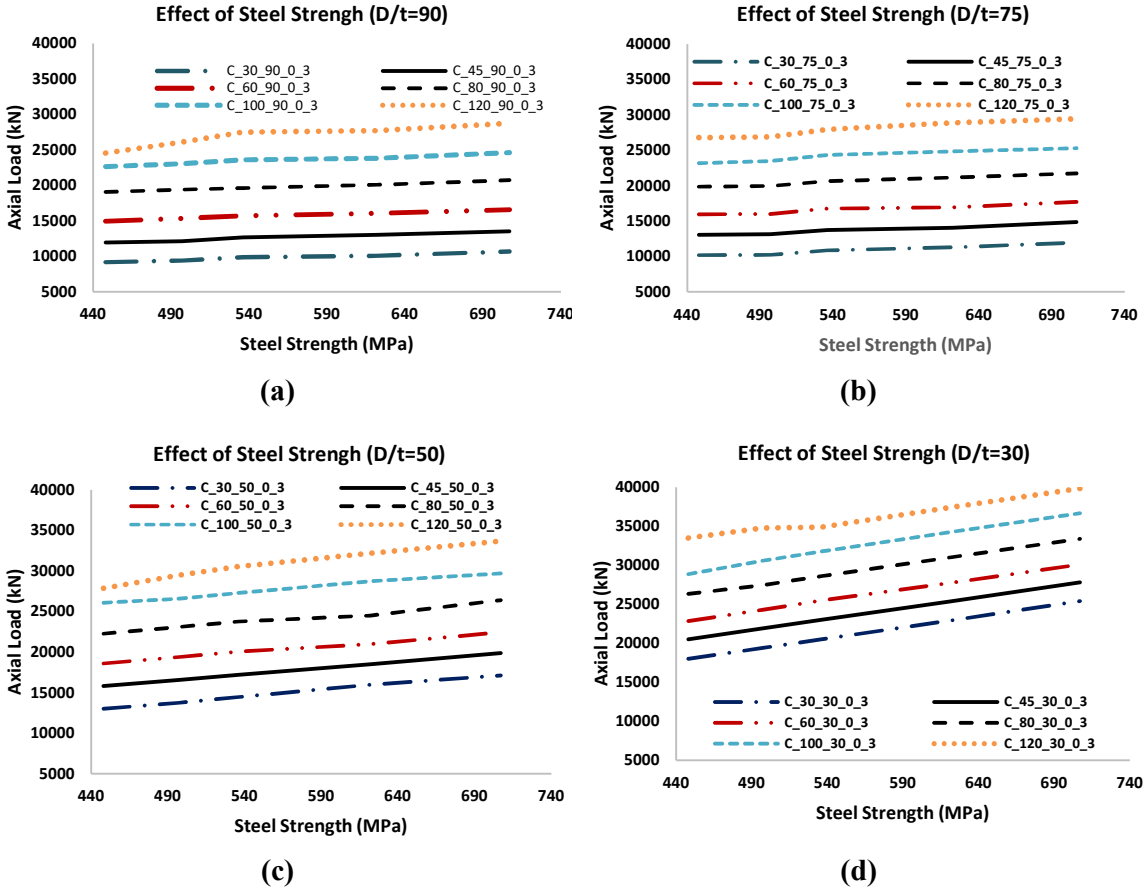

(a) (b)

(c) (d)

Figure 6.14: Effects of steel yield strength with concrete strength for different D/t, (a) D/t = 90; (b) D/t = 75; (C). (C) D/t = 50; (d) D/t = 30.

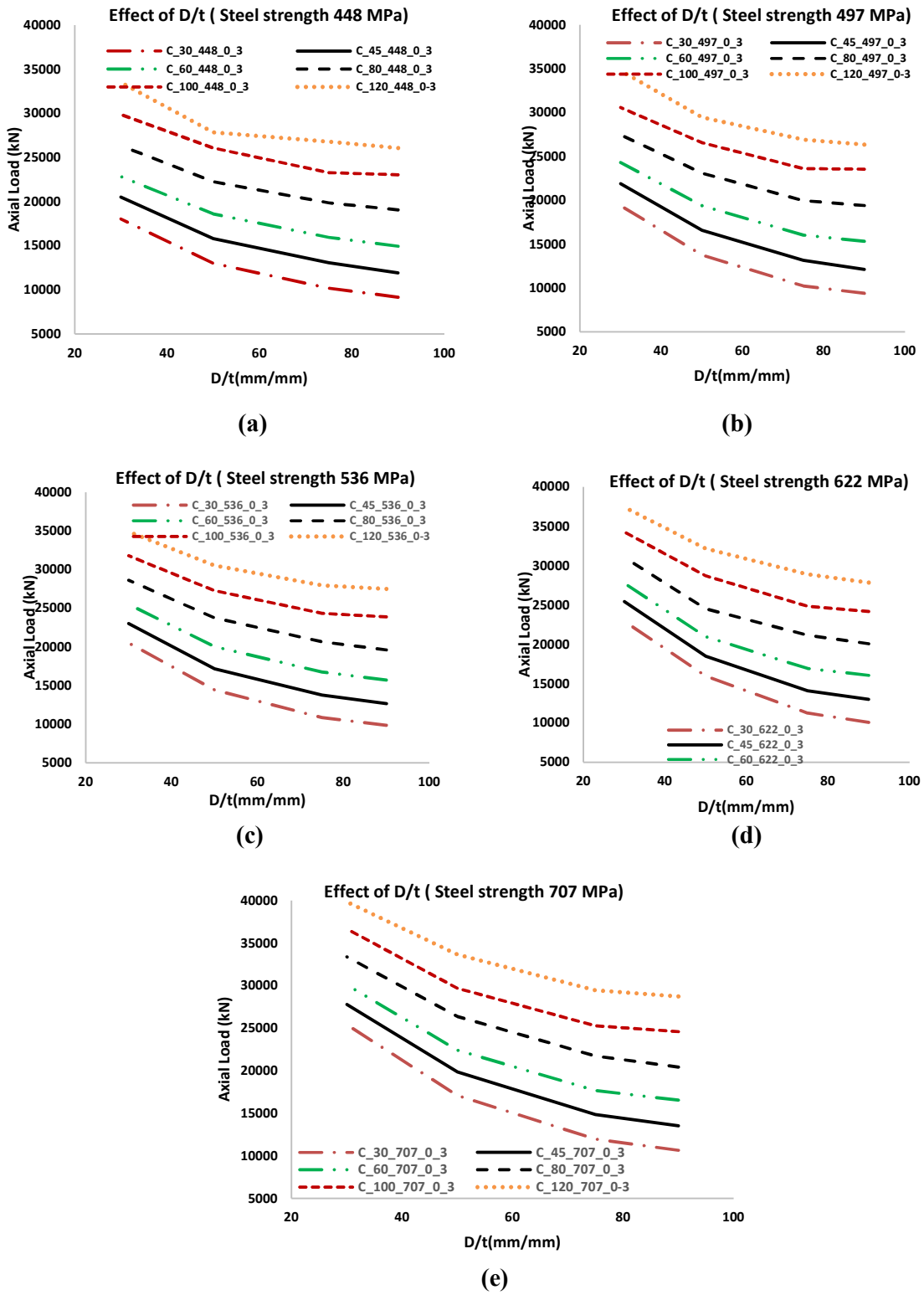

Figure 6.15: Effects of D/t ratio with concrete strength, (a) Steel strength 448 MPa; (b) Steel strength 497 MPa; (c) Steel strength 536 MPa; (d) Steel strength 622 MPa; (e) Steel strength 707 MPa.

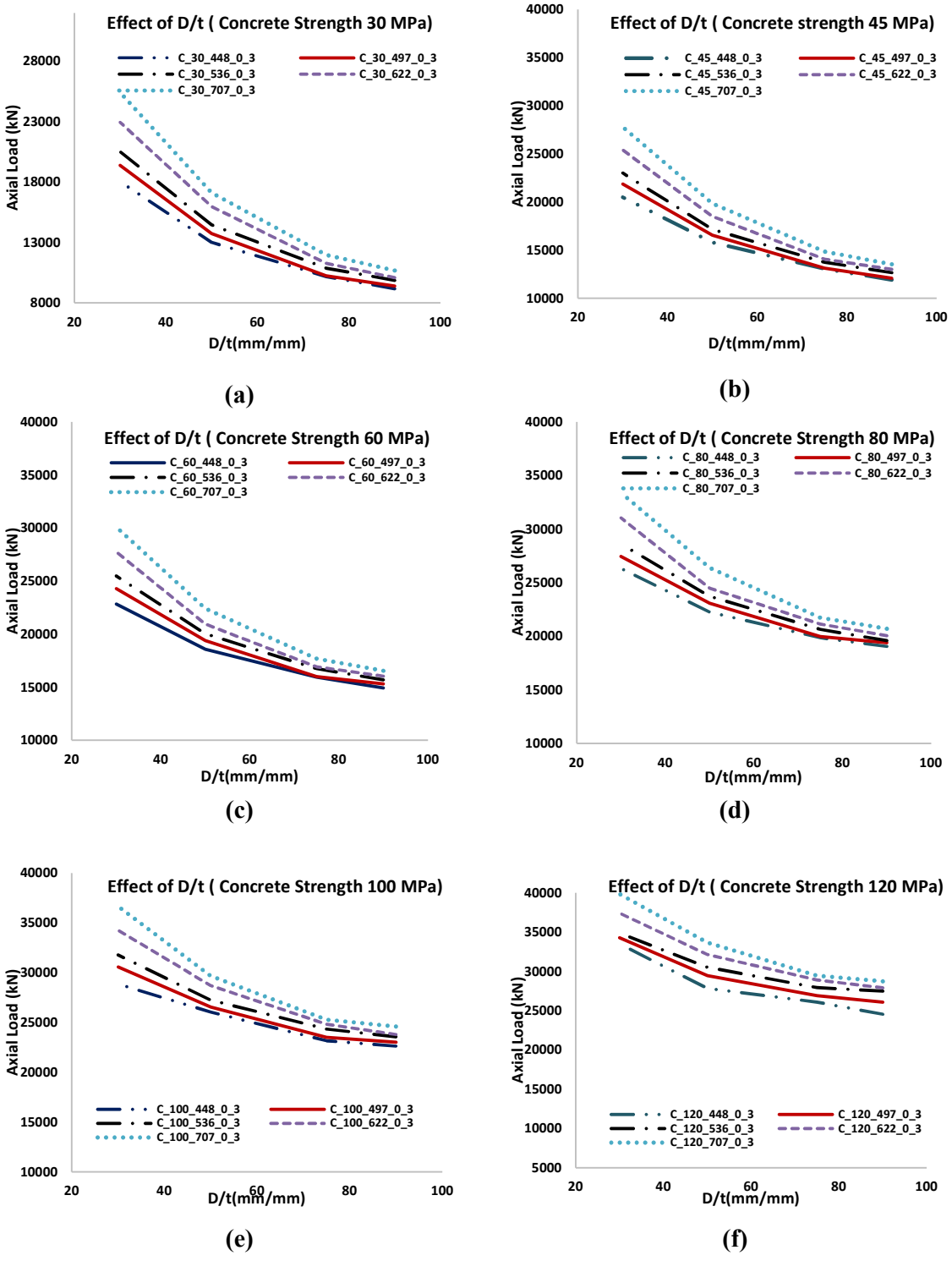

Figure 6.16: Effects of D/t ratio with steel strength, (a) Concrete strength 30 MPa; (b) Concrete strength 45 MPa; (c) Concrete strength 600 MPa; (d) Concrete strength 80 MPa; (e) Concrete strength 100 MPa; (f) Concrete strength 120 MPa

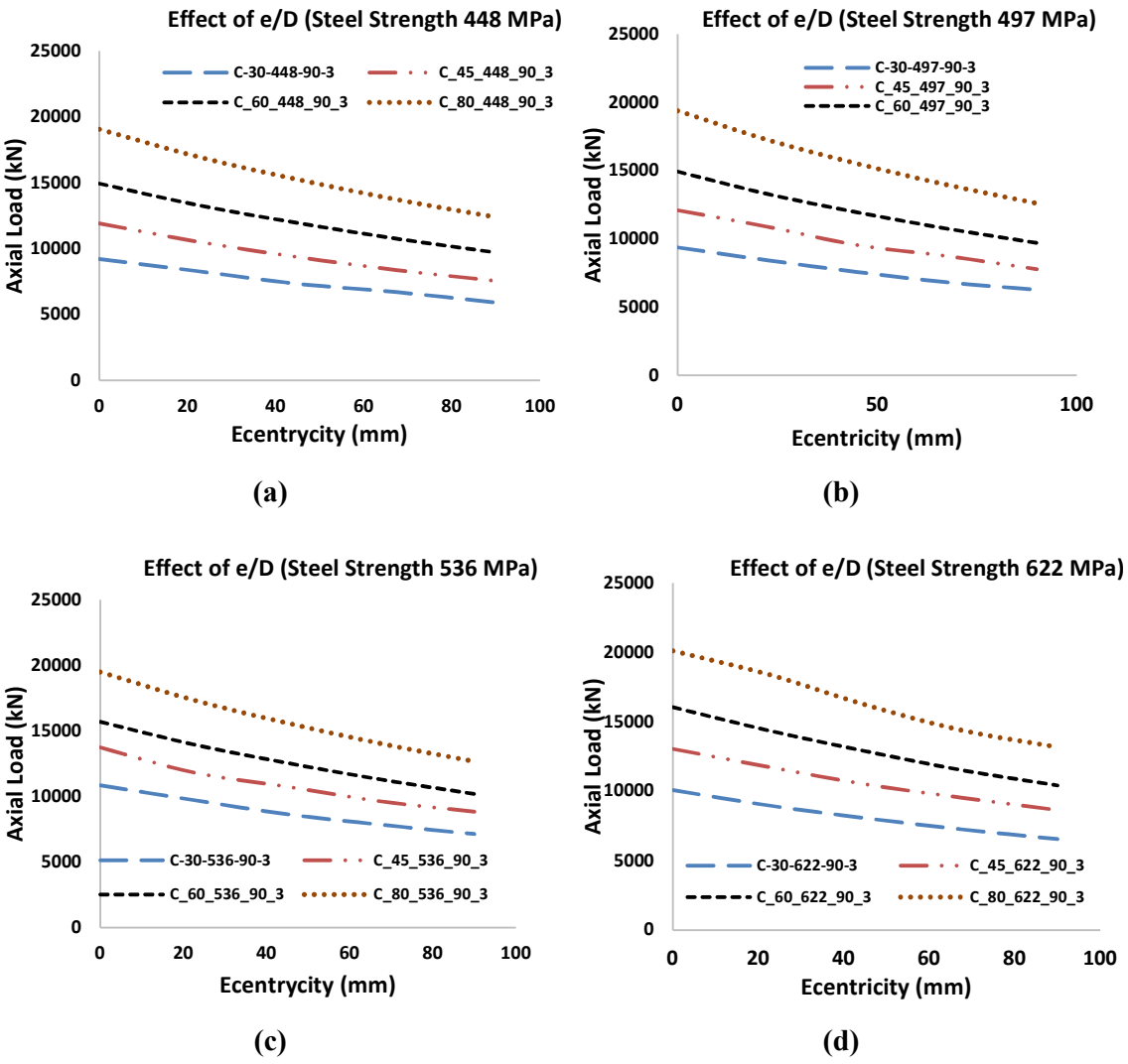

Figure 6.17: Effects of e/D ratio with concrete strength, (a) Steel strength 448 MPa; (b) Steel strength 448 MPa; (c) Steel strength 448 MPa; (d) Steel strength 448 MPa.

6.10 Proposed Design Rules

As the CFSST is the new concept of composite structure and complete design rules is yet to develop to predict the compressive resistance of CFSST column. According to the AISC (LRFD) steel construction, the compressive strength of axially loaded concrete filled composite column is $P_0 = A_s f_y + C_2 A_c f_c'$ where A_s is area of steel, A_c area of concrete, f_y is yield strength of steel, f_c' is the concrete compressive strength and value of C_2 is 0.85 for square/rectangular section and 0.95 for circular section. Stainless steel properties are different from the conventional carbon steel and the compressive strength of axially loaded

CFSST column would differ from that of carbon steel composite column. Concrete filled stainless steel column sections are not explicitly covered by the current design rules. So experimental test results obtained and extensive parametric study in the present study are compared with the existing design guidance of composite column the compressive resistance of axially loaded column can be expressed as $P_0 = A_s\sigma_{0.2} + (D/t)^{-0.014}A_c f_c'$ where A_s is the area of stainless steel, A_c is the area of concrete, $\sigma_{0.2}$ is the 0.2% proof strength of stainless steel, f_c' is the concrete compressive strength, t is the thickness of stainless steel section and D is the depth of column section.

Comparison between AISC ($P_0 = A_s F_y + C_2A_c f_c$' and current study ($P_o=A_sf_y + (D/t)-0.014A_cf_c$) prediction capacity of axially loaded composite column (FEC) with capacity found from FE simulation is as follows:

Table 6.6: Comparison of Proposed Prediction Formula with AISC Code & FE Results.

Parametric Specimens ID	A_s	A_c	P_{FE}	P_{AISC}	P_{CR}	P_{FE}/P_{AISC}	P_{FE}/P_{CR}
C45-448-90-0-3			11971	11392	12167	0.952	1.016
C-60-536-90-0-3	8900	193600	15694	14644	15677	0.933	0.999
C-80-448-90-0-3			19056	17152	18530	0.900	0.972
C-120-622-90-0-3			27992	25283	27349	0.903	0.977
C-45-448-75-0-3			13056	12112	12901	0.928	0.988
C-60-536-75-0-3	10656	191844	16748	15496	16547	0.925	0.988
C-100-536-75-0-3			24328	22018	23771	0.905	0.977
C-120-622-75-0-3			28904	26196	28299	0.906	0.979
C-45-497-50-0-3			16567	15029	16018	0.907	0.967
C-60-536-50-0-3			2007	18027	19110	8.982	9.522
C-100-622-50-0-3	15876	186624	28707	25738	27543	0.897	0.959
C-120-707-50-0-3			33668	30260	32426	0.899	0.963

Experimental Specimens ID	A_s	A_c	P_{EX}	P_{FE}	P_{CR}	P_{EX}/P_{FE}	P_{EX}/P_{CUR}
Sc_50.8x50.8	295.8	2284.84	223	217	226	0.973	1.013
SC_63.5x63.5	372	3660.25	356	331	348	0.930	0.978
SC_76.2x76.2	448.2	5358.24	423	393	414	0.929	0.979
SC_76.2x50.8	372	3498.96	299	298	307	0.997	1.027

From table 6.6 it is obvious that the proposed co-relation ($P_0 = A_s\sigma_{0.2} + (D/t)^{-0.014}A_c\ f_c'$) predicted capacity is very close to the FE results and experimental results for the wide range of both concrete (30-120 MPa) and stainless-steel strength (up to 750 MPa. So, limitation of concrete and steel strength could be overcome with proposed co-relation.

6.11 Conclusions

A detailed parametric analysis was performed to study the behaviour of CFSST columns subjected to concentric and eccentric axial loads. The influences were observed with respect to the peak axial load, failure mode and overall column load deformation responses. The findings of the study are presented as follows.

(a) The compressive strength of concrete has significant effect on the load caring capacity of CFSST columns. The axial capacity of CFSST column increased by 30%, 63%, 108%, 151% and 184% when the concrete strength increased from 30 MPa to 45, 60, 80, 100 and 120 MPa with steel grade of (448 MPa), respectively (AISC code predicted increments are 27%, 55%, 92%, 129% and 166%) For (707 MPa) grade steel the increment rates are 26%, 55%, 87%,130% and 169%, respectively (AISC code predicted increments are 22%, 44%, 73%, 102% and 132%).

(b) The yield strength of steel has also significant effect on the load caring capacity of CFSST columns. The axial capacity of CFSST columns increased by 3%, 7%, 10% and 16% when the steel strength increased from 448 MPa to 497, 536, 622 and 707 MPa with lower grade concrete (30 MPa), respectively (AISC code predicted increments are 5%, 9%, 17%, and 26%). For higher grade concrete (120 MPa), increment rates are 6%, 12%, 14% and 17%, respectively (AISC code predicted increments are 2%, 3.5%, 6.5%, and 9.5%).

(c) The axial capacity of CFSST column increased by 11%, 42% and 97% when the depth to thickness (D/t) ratio decreased from 90 to 75, 50 and 30, respectively.

(d) Higher eccentricity (e/D) ratio reduced the load carrying capacity significantly. The axial capacity of CFSST column decreased by 11%, 20%, 27% and 36% when the eccentricity (e/D) ratio increased from 0 to 0.05, 0.10, 0.15 and 0.20, respectively.

(e) Higher slenderness (L/D) ratio also reduced the load capacity significantly. The axial capacity of CFSST column decreased by 1%, 4%, 12%, 20% and 32% when the slenderness (L/D) ratio increased from 3 to 5, 7, 10, 15 and 15, respectively.

(f) The code (AISC-LRFD 2010) predicted capacity pattern were almost similar with numerical behavior but a bit conservative.

(g) Considering the load carrying capacity and behaviour from extensive parametric study, the compressive resistance for the CFSST square column can be expressed as the co-relation of $Po = A_s \sigma_{0.2} + (D/t)^{-0.014} A_c f_c'$ which shown very good accuracy.